Universidad Zaragoza
1542

Trabajo Fin de Máster

Estudio de la influencia de las tensiones tangenciales en el endotelio mediante un sistema microfluídico de placa de ateroma

Effects of wall shear stress on endothelial cells using an atheroma plaque microfluidic device

Autora

Itziar Ríos Ruiz

Directoras

Estefanía Peña Baquedano

Sara Oliván García

ESCUELA DE INGENIERÍA Y ARQUITECTURA
2019

AGRADECIMIENTOS

Después de un año de trabajo a veces duro, pero siempre maravilloso, me gustaría agradecer:

En primer lugar a Fany, por permitirme trabajar en algo tan apasionante lo primero. Y desde ese momento inicial, por todo el conocimiento que ha *intentado* transmitirme (¡a veces con éxito!), por el seguimiento incansable, la siempre necesaria guía y el optimismo. Así, la vida del investigador no es nada solitaria.

También en primer lugar a Sara, por su bendita paciencia, desde luego. Acoger a una ingeniera que no sabía ni ponerse un guante sin perder la paciencia ni la sonrisa es digno de mención. Gracias por todas las horas en campana y fuera de ella, por todo lo que he aprendido a nivel micro y macro.

A Miguel Ángel, también por darme la oportunidad de trabajar en este grupo, que es impresionante. Por todo lo que vamos a conseguir en estos años que quedan.

A todos los compañeros de laboratorio, pues siempre que he tenido cualquier duda han estado totalmente dispuestos a ayudarme y seguir enseñándome.

A todos los compañeros de la sala, por toda la ayuda y los ratos de dentro y de fuera de la uni.

A mis amigas y amigos, los de dentro que entienden mi trabajo y los de fuera que menos, pero se interesan de todas maneras. Pi, gracias por revisarlo todo como sólo tú sabes y por ser otra ingeniera en apuros en el laboratorio.

Por último, a mi familia. Richi, gracias por presentar el TFG tan simultáneamente, así la mayor atención/presión se ha centrado en ti (jiji). Bea, gracias por leerte una versión muy inicial y no volver a insinuar que te lo vuelva a pasar. Totalmente comprensible. Papá y mamá, gracias por estar siempre ahí, cada uno a vuestra manera.

ABSTRACT

Cardiovascular diseases are the main cause of death worldwide. Among them, atherosclerosis is the most common etiology. Atherosclerosis consists in the progressive narrowing of a blood vessel due to the deposition of an atheroma plaque. Despite the incidence of this disease, its mechanism is still not fully understood.

Studies have shown that atherosclerosis is a highly localised pathology. Therefore, it becomes clear that systemic factors in blood are not the only initiators of the disease. Locations more susceptible to develop atherosclerosis share disturbed flow patterns mainly due to the presence of bifurcations. Therefore, the biomechanics and haemodynamics of this pathology are increasingly gaining attention.

At cellular level, blood flow affects the endothelial cells in the vessel wall and influences their behaviour. Endothelial cells can modify their shape and orientation, resulting in an alteration of the vessel wall permeability. An increased permeability of the endothelium is the first step to develop atherosclerosis. Therefore, it is essential to study the effects of flow in cell shape and alignment.

This work has successfully developed a functional experimental test to study human coronary endothelial cells (HCAECs) and their response to blood flow. In particular, flow has been characterised by wall shear stress (WSS) or the tangential stress that cells experience due to blood flow. To do so, a microfluidic device has been designed and fabricated, the experimental protocol has been established and an image analysis program has been developed to postprocess the information obtained in the microscope.

Two batches of experiments have been carried out so far. Cell response in terms of shape and orientation to different values of WSS has been found in every case studied.

RESUMEN

Las enfermedades cardiovasculares son la principal causa de muerte en todo el mundo. Entre ellas, la aterosclerosis es la etiología más común. La aterosclerosis consiste en el estrechamiento progresivo de un vaso sanguíneo debido a la deposición de una placa de ateroma. A pesar de la elevada incidencia de esta enfermedad, su mecanismo aún no se conoce completamente.

La aterosclerosis es una patología localizada; por lo tanto, los factores sistémicos en sangre no son los únicos iniciadores de esta enfermedad. Las zonas más susceptibles de desarrollar aterosclerosis comparten patrones de flujo turbulento, debido principalmente a la presencia de bifurcaciones. Por todo esto, la biomecánica y la hemodinámica de esta patología están ganando cada vez mayor atención.

A nivel celular, el flujo sanguíneo influye en el comportamiento de las células endoteliales de la pared del vaso. Estas células pueden modificar su forma y orientación, provocando una alteración en la permeabilidad de la pared. Un aumento de la permeabilidad del endotelio es el primer paso para desarrollar aterosclerosis. Por lo tanto, el estudio del efecto del flujo en la forma y orientación celular es esencial.

En este trabajo, se ha desarrollado un ensayo experimental para estudiar las células endoteliales coronarias humanas (HCAECs) y su respuesta al flujo sanguíneo. En particular, el flujo se ha caracterizado mediante la tensión tangencial en la pared (WSS), tensión que experimentan las células debido al paso de la sangre. Para ello, se ha diseñado y fabricado un dispositivo microfluídico, se ha establecido el protocolo experimental y se ha desarrollado un programa de análisis de imágenes para posprocesar la información obtenida en el microscopio.

Hasta ahora se han llevado a cabo dos lotes de experimentos. Se ha encontrado respuesta celular en términos de forma y orientación a los diferentes valores de WSS en todos los casos estudiados.

Contents

Chapter 1

Introduction

The present study is focused on the biomechanics and haemodynamics of atherosclerosis, specifically at cellular level.

1.1 Description of the pathology

Nowadays, atherosclerosis remains one of the major causes of mortality worldwide. Despite its incidence, its mechanism is still not fully understood.[1] This pathology consists in the progressive narrowing of blood vessels, due to the deposition of an atheroma plaque in the vessel walls. The biggest risk of the formation of the plaque is that, under certain conditions, it can break and unleash a blood clot. This clot, also called thrombus, can travel throughout the circulatory system and finally occlude a smaller vessel, as can be seen in figure 1.1. Especially if this occlusion happens in the heart (myocardial infarction) or the brain (stroke), the consequences can be fatal. A brief description of the pathology is detailed hereunder.

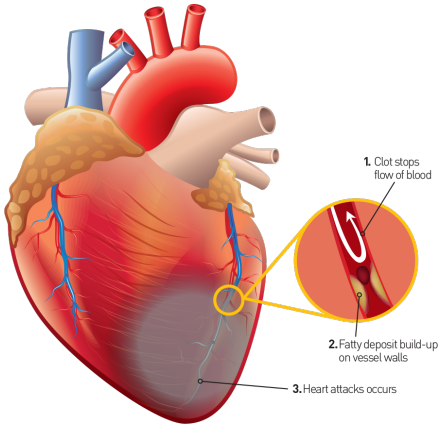

Figure 1.1: One of the possible outcomes of an atheroma plaque[2]

The mechanism of atherosclerosis is quite complex and involves many biochemical

and cellular procedures. Atherosclerosis commences with a dysfunctional endothelium. Toxins, mechanical damage or diabetes are some of the factors hypothesised to trigger this dysfunction. The damaged endothelium senses an increase in its permeability and consequently allows the leakage of macromolecules like low density lipoprotein (LDL) into the vessel wall.[3] These molecules accumulate in the intima, the most internal layer of blood vessels. The damage also triggers the inflammatory response cascade, involving the recruitment of monocytes.

Inside the endothelium, LDL oxidises, since it is no longer in the presence of the antioxidants in blood. The oxidation of LDL inside the wall provokes endothelial cells (ECs) to express some adhesion molecules and release cytokines.[3] The cytokines act as signaling cues that further increase the immune response, that is, the recruitment of monocytes. These monocytes, helped by the adhesion molecules, enter the vessel wall to eliminate the alteration - the oxidised LDL (ox-LDL). They differentiate into macrophages and start ingesting the ox-LDL via phagocytosis. The receptors of these immune cells do not receive any down-regulating signals and continue accumulating lipid until they transform into foam cells.[1]

Meanwhile, the muscle cells from the medial layer, with a contractile healthy phenotype, are altered because of the presence of ox-LDL. They change their phenotype and become smooth muscle cells (SMCs), with no contractile function, and migrate from the medial to the intimal layer. There, they surround the foam cells, generate an accumulation of extracellular matrix (mostly collagen) and form a fibrotic cap around the lipid core. The graphical scheme of the process is shown in figure 1.2. This accumulation is the atheroma plaque, and as it increases, it will damage the vessel wall with more severity and enter its lumen.

Several factors have been studied and some are currently acknowledged to influence the apparition of the disease, like dyslipidemia or the increased presence of LDL in blood. These factors are systemic, that is, they affect the whole circulatory system equally. However, atherosclerosis most frequently appears in specific locations, such as the carotid bifurcation, the coronary arteries, the infrarrenal abdominal aorta and the popliteal arteries.[1] What these sites have in common is that they involve bifurcations and areas where blood flow is disrupted or altered. For this reason, current research is focused on the haemodynamics and biomechanics that trigger this disease.

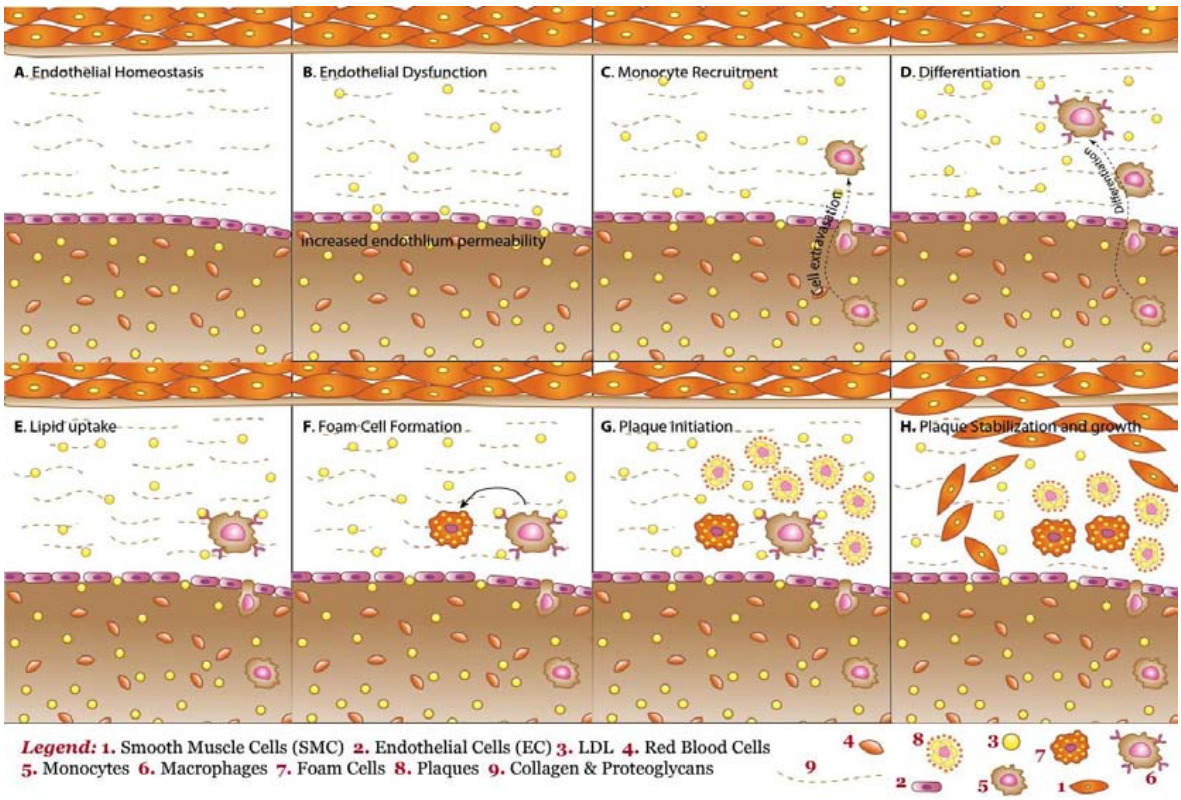

Figure 1.2: Process of formation of the atheroma plaque.[3] A blood vessel functions properly in homeostasis (A). When some factors provoke a dysfunction in the endothelium, its permeability is increased, and molecules in blood flow (like LDL) enter the vessel wall (B). The presence of these molecules generates a recruitment of monocytes (C), that different into macrophages inside the wall (D) and start digesting ox-LDL (E). When macrophages uptake too much lipid, they transform into foam cells (F), and stay inside the endothelium (G). The presence of these foam cells provokes a change in the phenotype of the muscle cells in the medial layer. They transform into smooth muscle cells and move to the intimal layer, where they surround the foam cells and generate collagen, stabilizing the forming plaque (H)

1.2 State of art

From the mechanical point of view, wall shear stress (WSS) or the tangential stress cells perceive due to the blood flow, has been the main parameter of interest to study. WSS is thought to be the main stress that affects wall permeability and, therefore, that initiates the formation of the atheroma plaque. It is perceived by cells in the endothelium through their mechanoreceptors, which allows them to respond to its stimulus.[1]

Therefore, several studies have tested the effect of different ranges of WSS in cell behaviour and wall permeability. Physiological and high WSS have been studied to be atheroprotective. On the other hand, low WSS causes a suppression of atheroprotective

genes and an over-expression of atheroprone one.[4] Some studies have found that areas susceptible to plaque formation are subjected to different shear stress waveforms than those atheroprotected. Implementing these WSS waveforms in the laboratory led to elongated and oriented cells when WSS was atheroprotective and rounded and with no preferred orientation when it was pro-atherogenic.[5]

To sum up, laminar and undisturbed flow patterns imply high and unidirectional WSS in the vessel walls. This WSS produces an elongation and alignment of the ECs in the direction of flow, which finally implies less permeability of the wall. However, in bifurcations and places were flow is disrupted, WSS becomes bidirectional, irregular and low. With these patterns, cells display a more rounded shape and no preferred alignment direction. This implies an increase in wall permeability, and subsequently, a bigger possibility to develop an atheroma plaque.

This dependency of cell shape and orientation on WSS has led many investigations towards the development of fluidic and microfluidic devices to simulate the different flow conditions.

One of the most common designs of microfluidic devices for atherosclerosis is the vertical-step flow system.[6] This device, displayed in figure 1.3, consists of a longitudinal channel where a step is included to reproduce the recirculation area generated after the plaque. With these devices, two areas of interest are found in only one experiment: the recirculation area above mentioned and a fully developed flow area, usually localised downstream the recirculation area. In both areas, WSS will show differences and so will the cells seeded in each of them. This type of devices has been used with human umbilical vein endothelial cells (HUVECs),[7] human aortic endothelial cells (HAECs)[8] and bovine aortic endothelial cells (BAECs).[9]

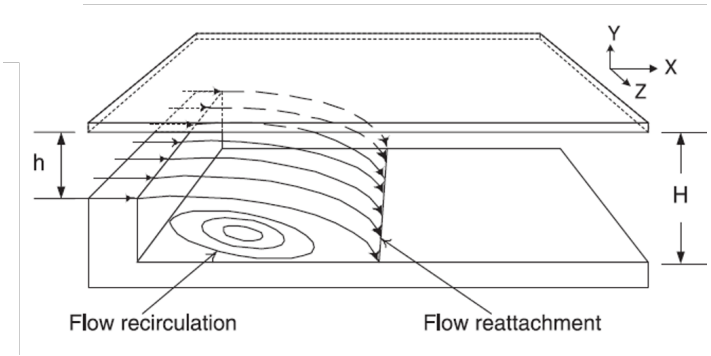

Figure 1.3: Scheme of a vertical-flow step device[6]

Another type of devices are the parallel-plate and the cone-and-plate shearing devices, see figure 1.4. Their mechanism is the same. Briefly, it consists of a culture plate where cells are seeded and a shearing cone or plate that applies the shear stress by rotating inside the culture medium. With this type of devices, the most common cell line tested is HUVECs.[5,10] Additionally, human coronary artery endothelial cells (HCAECs) are also studied with this device.[11]

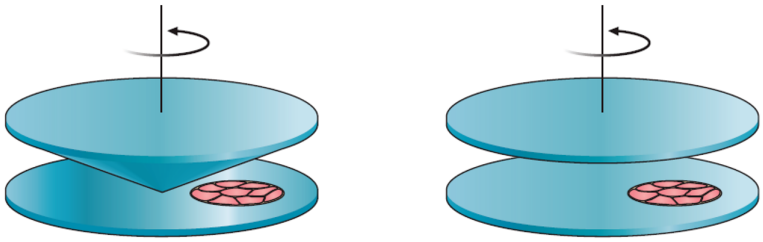

Figure 1.4: Scheme of cone-and-plate (left) and parallel-plate (right) shearing devices[6]

Other studies that develop microfluidic devices for studying atherosclerosis include the stretching of the substrate where cells are seeded. This is either to simulate the cyclic stretch in the arteries provoked by blood pressure[12] or to emulate the stenosed environment of the atheroma plaque.[13]

Although several studies have already correlated WSS and cell behaviour, it has become clear that depending on cell type, the threshold from which cells start to orientate is different.[14] For example, for ECs in the aortic artery, values of WSS of 1 to 8 Pa are reported to provoke morphological cell response,[15,16] whereas ECs in vein (HUVECs) show elongation and alignment in ranges of WSS around 0.1-0.3 Pa.[17,18] Therefore, it is interesting to study the cell lines of the vessels susceptible to suffer atherosclerosis. As commented above, HUVECs and HAECs (or BAECs) have been the most studied so far. Since the atheroma plaque also appears in the coronary and carotid arteries, apart from the aorta, this work will use human coronary artery endothelial cells (HCAECs).

Finally, it has also become clear that WSS alone cannot explain cell behaviour and plaque apparition.[19] There are other flow parameters, such as TAWSS (time-averaged WSS), OSI (oscillatory shear index) and RT (residential time), that show different patterns in areas where flow is disrupted.[20] The inclusion of these parameters is beyond the scope of this study. However, it is one of the future lines of this research.

1.3 Objective

As commented above, atherosclerosis begins when the permeability of the vessel wall increases. Therefore, it is crucial to fully understand the mechanisms that trigger this dysfunction in the permeability, which is correlated to ECs shape and orientation.

It is then the main objective of this work to analyse HCAECs response to WSS, regarding cell alignment and orientation. To do so, three main areas have been addressed in this study: the design of the microfluidic device that would reproduce the required test conditions, the *in vitro* tests and the postprocessing of the information obtained in these experiments. Each area was a new challenge, so it entailed a background analysis and a careful implementation. Different protocols have been defined and followed in order to ensure the repetitiveness and validity of the tests. Each procedure and its related subactivities are described in the following chapters.

This is the first step of a larger investigation that will also involve the study of cell response to a different stimulus, strain, and to coupled stress-strain stimuli.

The tasks and procedures were carried out in the University of Zaragoza, in the Applied Mechanics and Bioengineering (AMB) group of the Aragon Institute of Engineering Research (I3A).

Chapter 2

Design and fabrication of the microfluidic device

2.1 Requirements, initial device and modifications

The first step is to design the microfluidic device. To do this appropiately, it is essential to clearly define every condition that it will have to reproduce. As this work studies cell response to WSS alone, decoupled from other mechanical stimuli (strain in particular), the substrate where cells will be seeded must be rigid. Additionally, in order to obtain complete response results, cells must be subjected to a wide range of shear stresses, reaching values below and above the physiological level. Considering that the physiological WSS in the coronary arteries is 0.68 Pa,[21] the device will have to be able to withstand WSS up to 1 Pa.

Originally, this work planned to use a microfluidic device that had already been used by the research group for different flow tests. It consists of three squared channels 2 mm wide, 2 mm high and 35 mm long, with a cylindrical entrance of 2.3 mm in diameter. The total dimensions of the device are 15 mm (W) x 40 mm (L) x 6 mm (H). It is made of polydimethylsiloxane (PDMS), due to its studied biological properties (non-cytotoxicity mainly). The mould to generate these PDMS devices is made of a biocompatible resin (Clear) and manufactured with a 3D printer using stereolitography technique (SLA or SL) by the company Beonchip S.L. Finally, it is attached via plasma treatment to a microscope slide, where cells will adhere and grow, see figure 2.1. Therefore, the requirement of a rigid substrate is already met by this initial design.

To supply the flow to the system, a peristaltic pump is used. Its main advantage is that the flow is never in direct contact with the pump, facilitating the sterility of the process. In particular, the pump used is Watson-Marlow, model 323S, with a 318MC

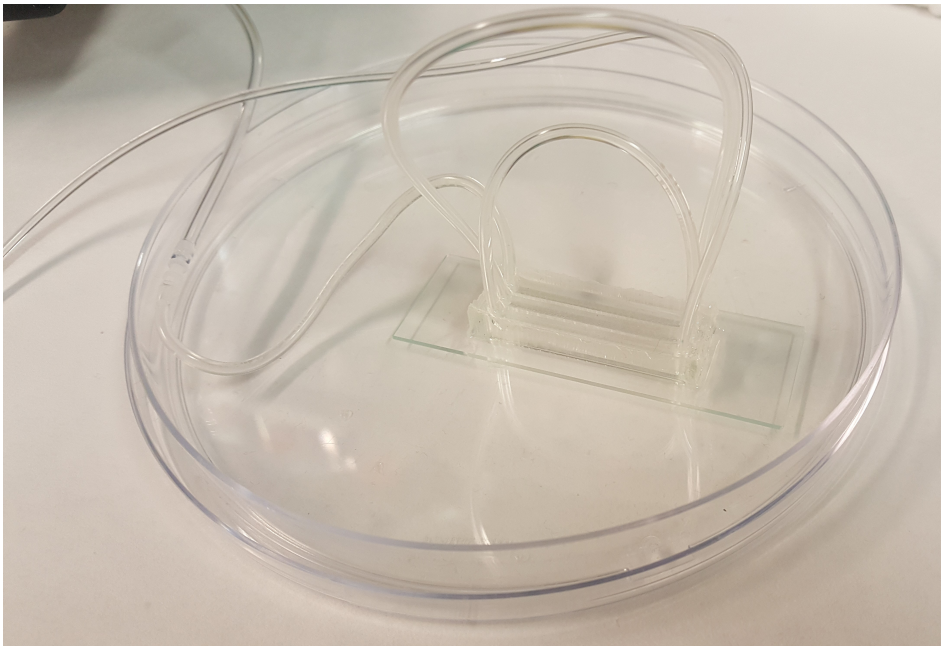

Figure 2.1: Set up of the initial device, attached to the microscope slide. It consists of three channels, connected among each other with the tubing system. These tubes come from the peristaltic pump, which will provide the flow rate

pumphead, see figure 2.2. The head's maximum speed is 110 rpm. The flow rate supplied by this speed depends on the diameter of the tube around the head. With the widest tubes in the laboratory, the maximum flow rate achievable is 10 ml/min.

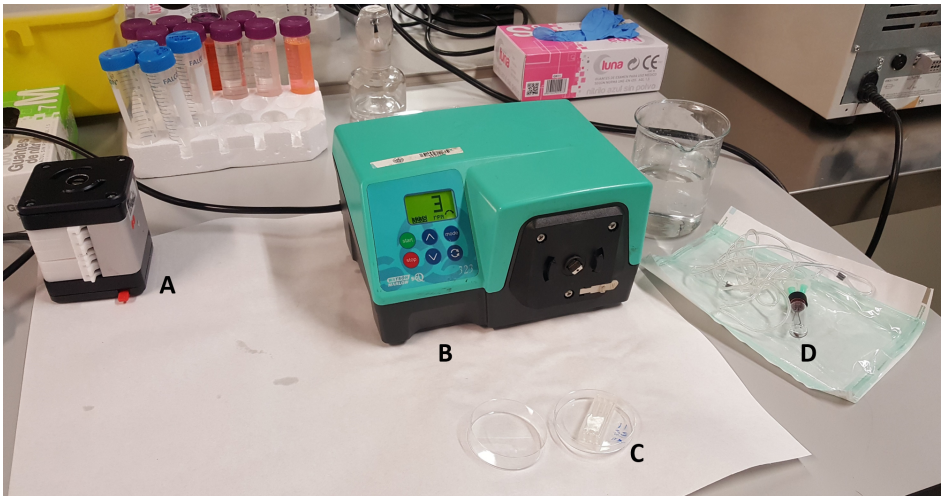

Figure 2.2: Whole flow system. B and A are the peristaltic pump and the pumphead, respectively. C is the microfluidic device and D indicates the set of tubes and the fluid deposit for the experiments

Considering this initial design, several simulations were computed to determine the test conditions required to generate the desired flow parameters. These simulations were run in the commercial software Comsol. Since large deformations in the device are

expected, fluid-structure interaction (FSI) was performed, instead of computational fluid dynamics (CFD), as this last methodology only studies the fluid. FSI considers the deformation that the fluid (in this case, the culture medium) causes in the solid (the PDMS device) due to the pressure it exerts on it. The calculus is then updated with the deformed geometry of the solid and the whole system is recalculated, until the equilibrium is reached. Therefore, to properly define the FSI simulation, both the PDMS and the culture medium must be fully characterised. Both material characterisations are described in sections below.

With these FSI simulations, it was obtained that the highest possible flow rate generated a WSS of only 0.9 Pa, see figure 2.3. As the tests required higher levels of WSS, this device would not be valid for the study.

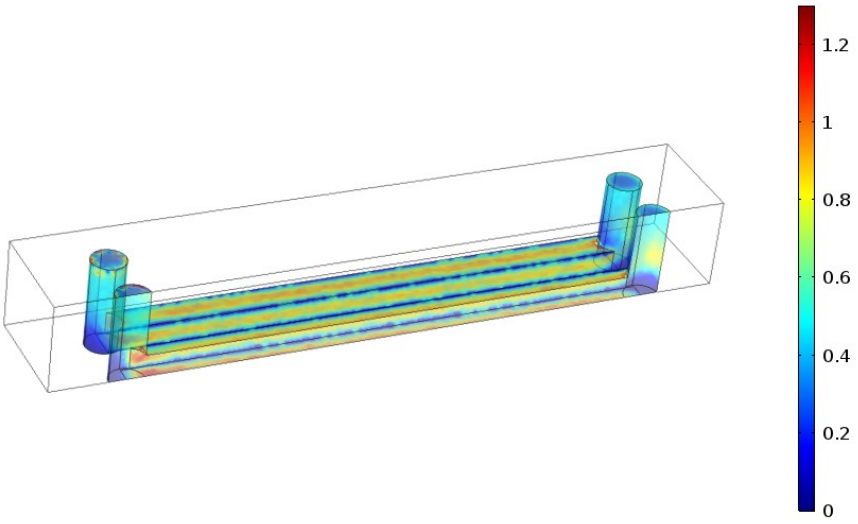

Figure 2.3: Representation of the initial microfluidic device in Comsol. Only half of the geometry is simulated due to the symmetry of the device. Scale colour bar of WSS (Pa) when it is subjected to a flow rate of 10 ml/min

In parallel, several trials were carried out in the laboratory to check the device and some test parameters (such as outlet pressure), see figure 2.4. In these tests, a different flow rate limit was met, since the system could not bear rates above 6 ml/min given the reduced channel area. Over 6 ml/min, which corresponds to a WSS of 0.39 Pa, the device would be compromised and the cells would detach.

Following these restrictions, the need for an updated design of the device emerged. The goal is for it to be able to reproduce a WSS of 1 Pa, always considering the limitation of a flow rate of 6 ml/min. The only geometrical restriction is to maintain

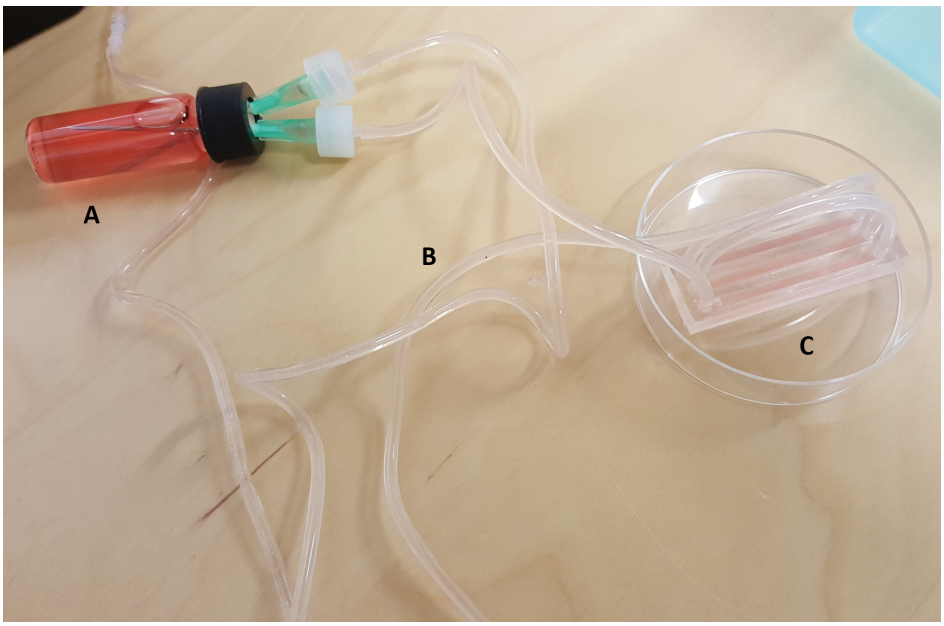

Figure 2.4: The initial device (C) with the tube montage required for the tests (B) and the fluid deposit of 5ml (A). MesoEndo Cell Growth Medium is already present through the whole system

the diameter of the inlets and outlets, as it matches the tubes in the laboratory.

WSS is directly proportional to the shear rate, as shown in equation (2.1). τ_w represents the WSS (Pa), η is the dynamic viscosity (Pa·s) and γ is the shear rate (s^{-1}). The shear rate, defined in equation (2.2), is the velocity gradient or the change in velocity in which a layer of fluid moves with respect to another. v is the relative velocity of the moving plate (m/s) and h is the distance between the layers (m).

$$\tau_w = \eta \cdot \gamma \tag{2.1}$$

$$\gamma = \frac{v}{h} \tag{2.2}$$

Since the substrate remains static, higher fluid velocity subsequently implies higher WSS. As the flow rate has an operational limitation, the way of increasing fluid velocity is by reducing the cross-sectional area of the channels. The width of the channels was decided to be maintained, in order not to reduce the area where cells will be seeded. Finally, with the aim of having two different values of WSS per test, an inverse step was proposed to reduce the cross-sectional area in the final half of the channels, as

shown in figures 2.5 and 2.6.

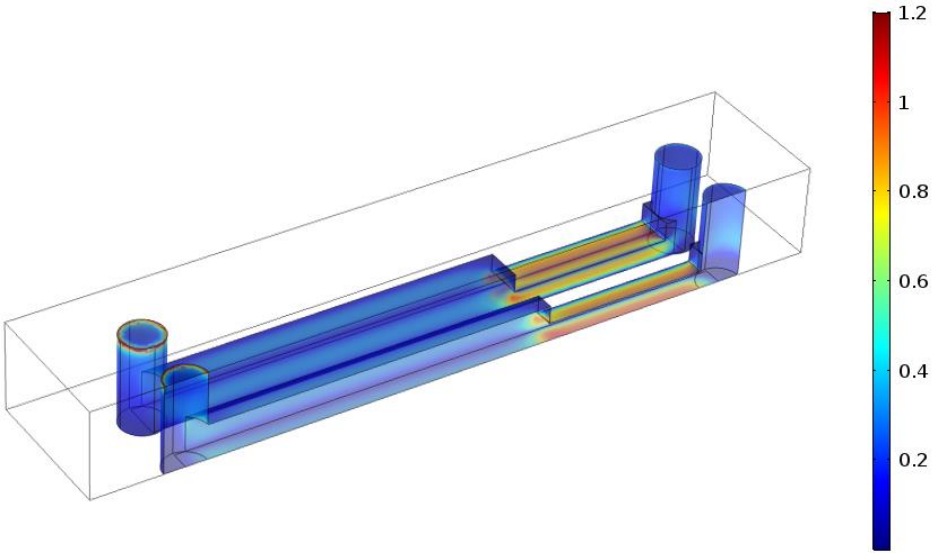

Figure 2.5: Representation of the final geometry of the device in Comsol. There are two areas with distinct WSS (Pa), shown in the colour bar. WSS of 1 Pa is reached in the downstream area with a flow rate of 4.5 ml/min. Flow direction is from left to right

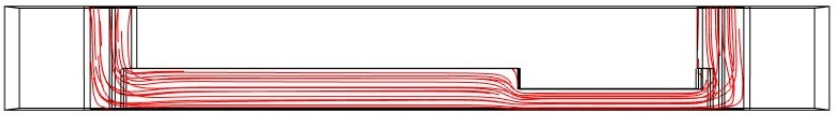

Figure 2.6: Streamlines in the longitudinal section of the final geometry. The possible flow disturbance due to the presence of the inverse step would not affect the cells seeded. Flow direction is from left to right

Considering this modification, a WSS of 1.44 Pa is reached with a flow rate of 6 ml/min, a value beyond requirements.

2.1.1 PDMS characterisation

For the FSI simulations, the mechanical properties of the PDMS were needed. The characterisation of the material was carried out following a standard that specifies the procedure to determine tensile properties of this type of material. Specifically, the method followed the indications given in ASTM D638-14 Tensile Properties of Plastics,[22] in order to determine the modulus of elasticity and Poisson's ratio.

A total of 8 test specimens were machined according to the standard, to make sure to have enough valid tests.

The tests were carried out in the Tissue and Biomaterial Characterisation Laboratory, in the Aragon Institute of Engineering Research (I3A), using the test machine Instron 5848. The tests used a video extensometer to measure both the axial and transverse strain simultaneously. Figure 2.7 shows the specimen between both clamps, with the four dots in the center that will be followed by the video extensometer for the axial and transverse strain.

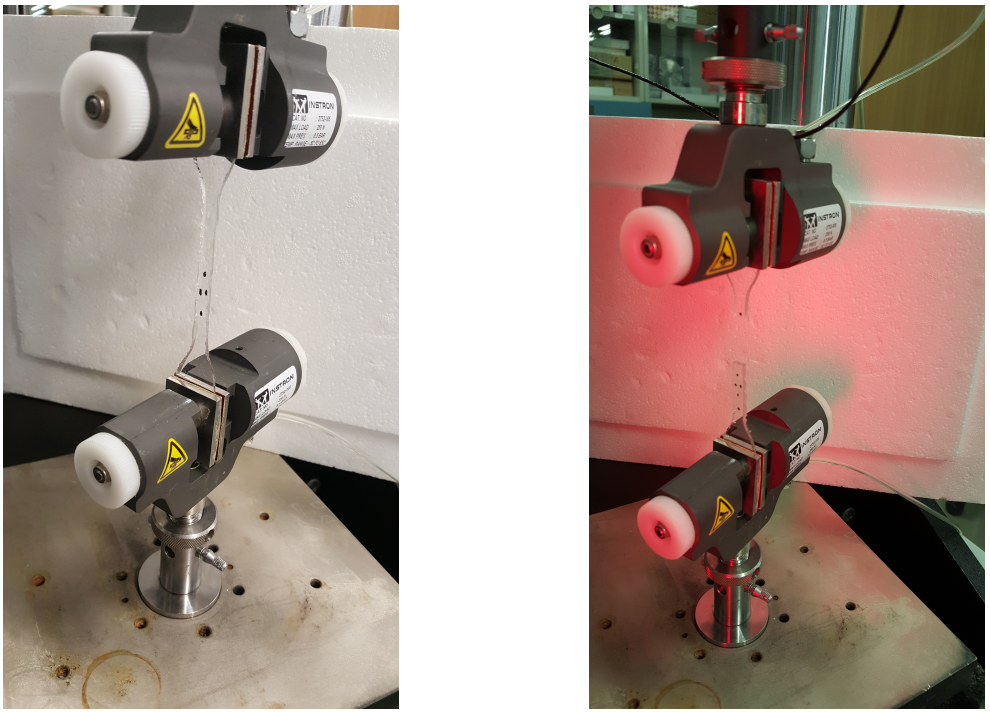

(a) Disposition before the beginning of the test (b) End of the uniaxial test

Figure 2.7: Uniaxial test performed to the PDMS specimens, following ASTM D638-14

The procedure works as follows: a small preload of 0.2 N is applied at a crosshead speed of 0.1 mm/min, according to standard. Afterwards, the test speed is set to 5 mm/min, with a working bench of 10 N to show precision at small strains. Once the tests are finished, the data are imported and post-processed to obtain the desired parameters. Due to the compliance of the material, the tests produced large deformation in the specimens. Therefore, the initial linear portion had to be localised in order to calculate Young's modulus. The American standard is not specific in defining what to consider the linear portion of the curves. Therefore, the Spanish standard UNE-EN ISO 527-1[23] was consulted as guideline for this particular

requirement. According to it, the strain interval between 0.05% and 0.25% must be the portion chosen as the initial linear segment, and thus, where the slope is calculated to obtain the elastic modulus, as shown in figure 2.8.

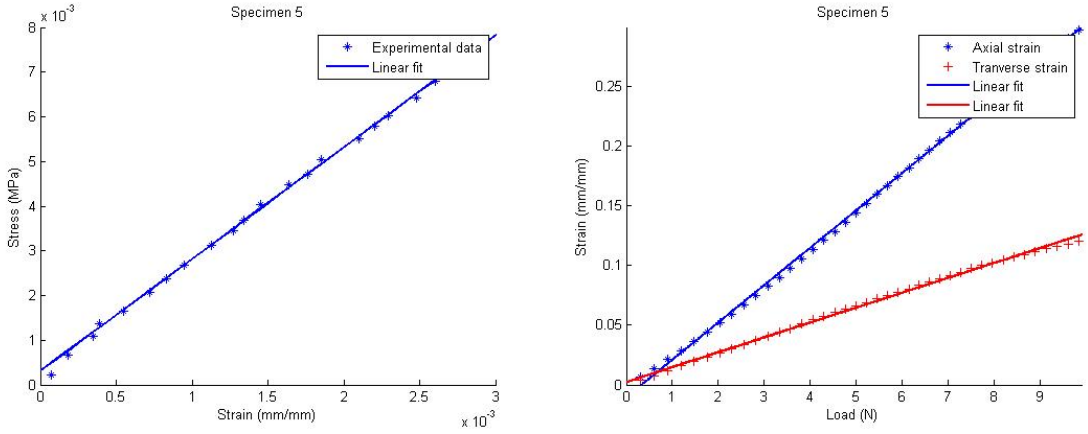

(a) Experimental data and numerical fit of the axial stress-strain curve. This linear fit allows the obtention of Young's modulus

(b) Experimental data and numerical fit of the axial and transversal strain represented vs the load. With these fits, Poisson's ratio is calculated

Figure 2.8: Postprocessed results of the uniaxial test of the specimen 5

After postprocessing all data, a variability in the results was found. These differences split the results into two groups, which matched two slightly different polymerization processes. Two specimens were machined out of a material that was cured right after mixing the PDMS with the crosslinking agent. The remaining mixture was kept at -20ºC and, once needed for the other batch of specimens, cured for 24 hours at 60ºC. This intermediate freezing process significantly affected the material properties.

Considering this variation and in order to homogenise the mechanical properties, the protocol of PDMS fabrication for the devices was decided to include at least an overnight storage at -20ºC.

After the calculation of Young's modulus and Poisson's ratio, these are transformed into the Lamé parameters, following equations (2.3) and (2.4). These parameters are necessary since PDMS is modelled by the Neo-Hookean hyperelastic model and the parameters in this model are related to the Lamé parameters. Table 2.1 shows the parameters that define the behaviuor of the material.

$$G = \frac{E}{2 \cdot (1 + \nu)} \tag{2.3}$$

$$\lambda = \frac{\nu \cdot E}{(1 + \nu) \cdot (1 - 2 \cdot \nu)} \tag{2.4}$$

Table 2.1: Elastic and Lamé parameters obtained in the characterisation of the PDMS. Mean and standard deviation are shown for the Young's modulus and Poisson's ratio. Lamé parameters were calculated with their mean value

E (MPa)	ν	**G (MPa)**	λ **(MPa)**
2.59±0.3	0.39±0.012	0.93	3.45

2.1.2 Culture medium characterisation - Addition of Dextran

Along with the PDMS properties, the rheology of the culture medium is also an important factor for the design of the microfluidic device. The medium used for these tests is MesoEndo Cell Growth Medium (212-500) from Sigma-Aldrich. It is suitable for endothelial cells, including HCAECs used in this study.

The parameters of interest are the density and the dynamic viscosity of the fluid. Supplier specifications of the product do not include these characteristics. Therefore, the rheological analysis has to be performed separatedly.

The density of the product is easily measured in the laboratory. However, its dynamic viscosity needs a viscosimeter or rheometer to be obtained. These measurements were carried out in the Service of Rheological Characterisation of Fluids of the University. There, a rheometer with a cone-plate sensor is used (from Haake, model RheoStress1), to allow more accurate measurements for low viscosity fluids (of around 1 mPa·s, the viscosity of water) and to need less sample quantity. In particular, each measurement required 0.5 ml of sample.

Firstly, the culture medium with no alterations was measured. The fluid presented a dynamic viscosity of around 0.95 mPa·s (see figure 2.9). This value is way below blood's viscosity, 4-4.5 mPa·s.[24]

In order to mimic more closely the physiological environment, it was decided to increase culture medium viscosity. This is achieved by the addition of Dextran D4876

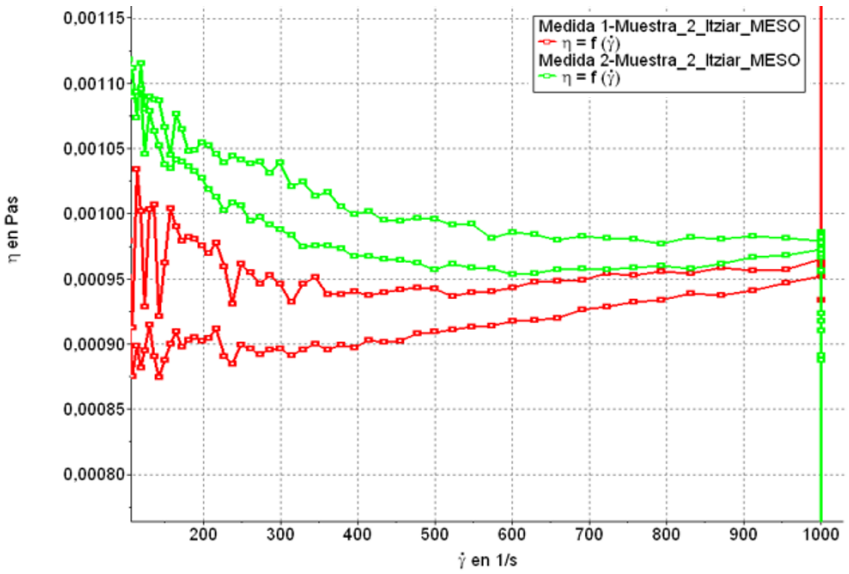

Figure 2.9: Viscosity vs shear rate of MesoEndo Cell Growth Medium (Sigma-Aldrich). Measurements of two different samples

(MW 150,000 by Sigma-Aldrich), a soluble compound that has been broadly used in other studies in literature for that purpose.[25–27] It is reported to not alter cell behaviour, specifically in the parameters of interest of this study.[28,29]

Therefore, the quantity of Dextran needed to obtain a dilution with blood viscosity was estimated and checked.[30] The final solution includes 4.93% (w/v) of Dextran.

Once Dextran is added, the solution must be subsequently filtered with a 0.2 μm Nylon filter to remove any possible contamination that may have occurred during the mixing process. This final solution presented a dynamic viscosity of 3.9 mPa·s, as shown in figure 2.10.

2.2 Mould design and fabrication

Once the final geometry of the device was established, the mould to make it had to be designed. The software Solid Works was used to create the mould. Due to the need of fast response, all trials were manufactured in a 3D printer as well (Lion2 by Leon 3D), but using Fused Deposition Modelling (FDM) technique, in the Design Engineering and Manufacturing Department of the University. Several prototypes were tried to ensure the required dimensions of the microfluidic device (anticipating moulding shrinkage), as a small variation can be crucial in the performance of the device.

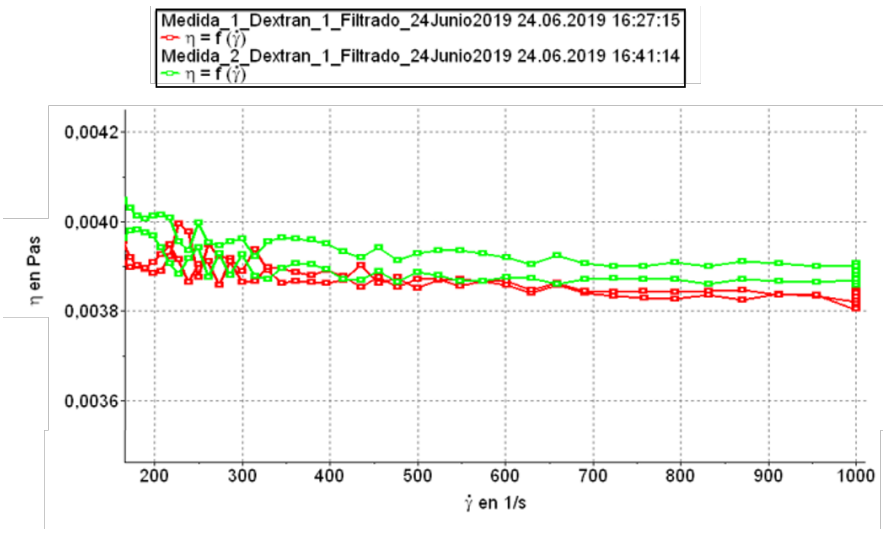

Figure 2.10: Viscosity vs shear rate of the prepared solution of MesoEndo Cell Growth Medium and 4.93 % of Dextran (both from Sigma-Aldrich). Measurements of two different samples. The flatness of the curves indicates that the fluids can be considered newtonian

An additional modification in the mould was the incorporation of a draft angle, to facilitate the demoulding. After checking in the FSI simulations that this angle did not imply any changes in the test conditions, a draft angle of 15º was included in the female part. The design of the new mould is represented in figure 2.11

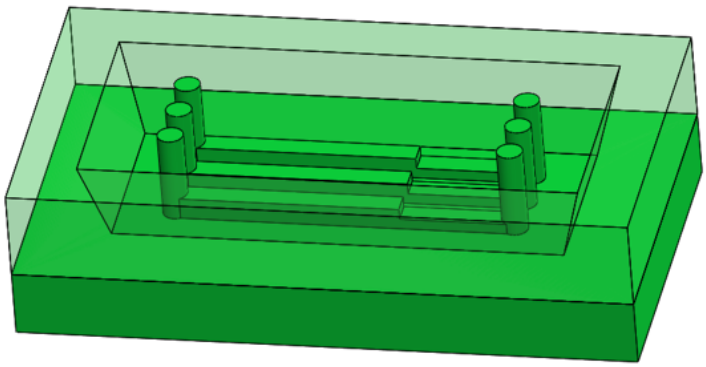

Figure 2.11: Final and assembled geometry of the mould in Solid Works. Female part represented translucent to allow visualization of the channels geometry

Regarding the material of the mould, as it is different form the commercial moulds of the initial device, a viability analysis was carried out. The main requirement is that no mass exchange takes place in the oven while curing the PDMS, to avoid any cytotoxicity possible. Initially, the studied material was acrylonitrile butadiene styrene (ABS), one of the most common thermoplastic polymers used in FDM 3D printers.[31] Although ABS is considered biocompatible,[32] cytotoxicity tests were also performed

on this material, with good results. Polypropylene (PP) was also considered as mould material considering its widely known biocompatibility. However, the cytotoxicity tests gave inconclusive results. Therefore, ABS was chosen as mould material for the trials prior to the final design.

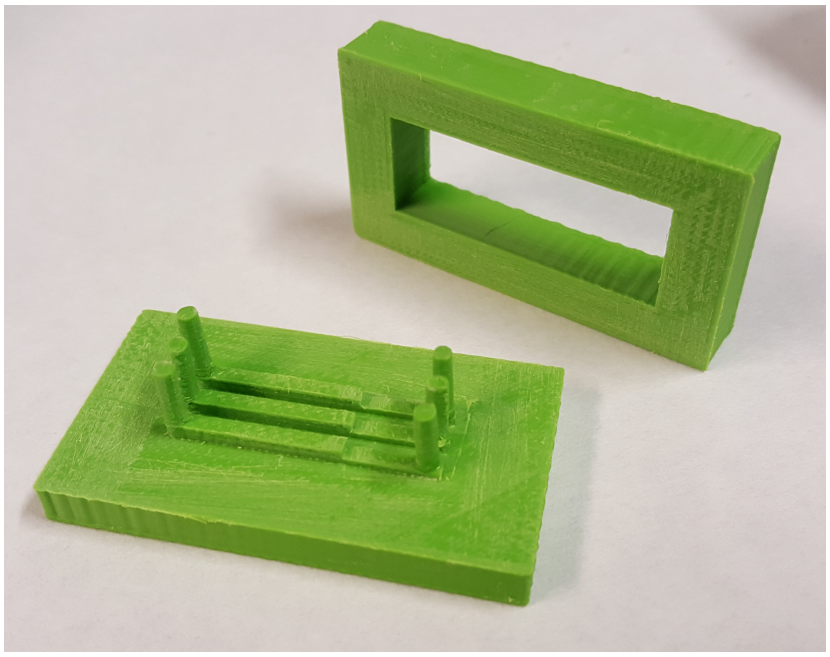

Figure 2.12: ABS mould showing high roughness. Sandpaper was used to reduce this roughness, but the precision acquired was not enough for the devices

Apart from the material itself, the moulds fabricated with FDM presented higher roughness, which translated to the device and its channels, as can be seen in figure 2.12. Research on how this roughness can affect the cells in the device was performed. Supposedly, the effect would be negligible.[33] However, cell behaviour was unexpectedly altered. Therefore, the final mould geometry was sent to Beonchip to be elaborated with the same resin as the initial one, figure 2.13.

2.3 Fabrication of the microfluidic device

The fabrication of the microfluidic device involves the preparation of the PDMS and its curing in the mould.

PDMS is supplied from Dowsil as a Silicone Elastomer Kit. This kit includes the silicone elastomer base and the curing agent. These two components are mixed in proportion 10:1 in weight. The blend is then stirred and kept at -20ºC. As the

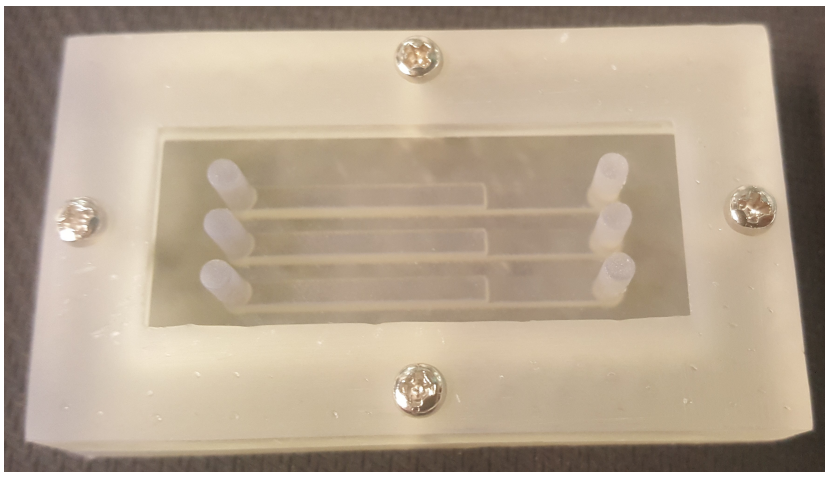

Figure 2.13: Final mould made of a biocompatible resin by stereolitography, used for the fabrication of the final devices

material is more rigid after kept cold and in order to make larger batches of PDMS, it was decided to use it after storage.

Once the PDMS is prepared, it is poured into the mould and the air is removed in the vacuum machine. Afterwards, it is left to cure at 60°C overnight. Finally, it is removed from the mould and bonded to the microscope slide using plasma treatment and a supportive overlay of PDMS. This procedure is a standardised protocol in the laboratory. The final device is shown in figure 2.14

It is mandatory to sterilise the devices before any contact with living cells. This sterilsation is carried out in the autoclave (from JP Selecta, PV-1157), at 120°C for 20 minutes.

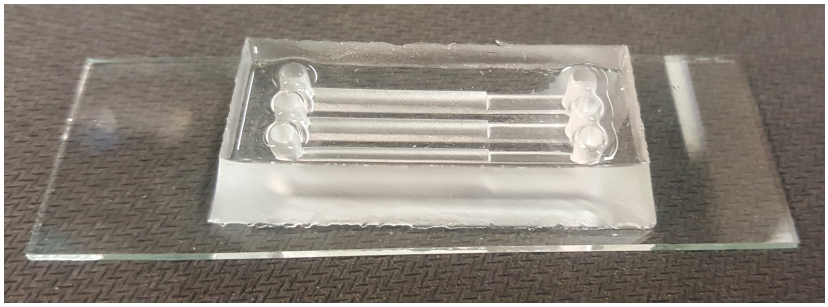

Figure 2.14: Final microfluidic device. The cross-sectional area reduction can be seen in the right part of the three channels. Culture medium will flow from left to right

Chapter 3

In vitro testing

This section describes all the protocols followed in the laboratory. It is crucial to follow every procedure carefully, as sterility is easily compromised. It should be noted that every operation here described that involves cell manipulation and exposure must be conducted inside a laminar flow hood (Telstar, Bio II A).

3.1 Cell seeding and system tuning

Before seeding, the glass substrate of the microfluidic device needs to be treated to enhance cell adhesion. Thus, a dilution of 0.1 mg/ml of rat tail type I collagen (Corning, ref. 10224442, Fisher Scientific) is prepared and distributed along the channels of the device, where cells will attach and proliferate. The chip is afterwards left for 30 minutes in the humidified incubator,[34] at 37ºC and 5% CO_2 (ThermoFisher Scientific, HeraCell 150i). During this timelapse, cell subculture will be prepared. Afterwards, the solution in the channels is aspired and the device is carefully washed with PBS (ref. 17-516F, Lonza) to remove any traces left.

HCAECs have been previously cryopreserved in liquid nitrogen in vials, each containing 1 million cells suspended in culture medium and a cryoprotectant, dimethyl sulfoxide (DMSO, ref. 276855, Sigma). Once needed, a cryovial is submerged in a 37ºC water bath. Right before the cells are completely thawed, it is removed from the heat and its content is resuspended and introduced in a flask containing cell medium. The flask is afterwards introduced in the incubator, which maintains an atmosphere of 37ºC and 5% CO_2, for cell growth. Whilst left to grow, cell medium must be refreshed every 48 hours. Once cells have reached high confluence they will be seeded in the microfluidic device.

To obtain the cells that are attached in the flask, they must be trypsinized. For this, it is first necessary to remove the medium by aspiration. Cells are subsequently rinsed in PBS to the medium, as it inhibites the action of trypsin. Subsequently, the solution of trypsin/EDTA, ref. CC-5012 from Lonza, is poured into the flask. The flask is afterwards left for 2 minutes at room temperature to make the cells detach from the flask. Once this detachment is verified by visual checking in the optical microscope, the flask is filled with cell medium to prevent further action of the trypsin, as it could irreversibly damage the cells.

This mixture is later centrifuged for 5 minutes at 1200 rpm in the centrifuge 5810 R from Eppendorf. Afterwards, the supernatant is aspired and the remaining pellet of cells is resuspended in 1 ml of medium by gently pipetting to break up the clumps.

Once cells are resuspended, they are counted in a hemocytometer in order to know the cell density injected in the channels of the microfluidic device. Depending on the obtained number of cells per milliliter, the resuspension will be modified to provide around 100,000 cells per squared centimeter[7,35,36] (the device has a total seeding surface of 1.8 cm^2).

(a) Overview of the hemocytometer. The glass slide is placed over the central part of the device

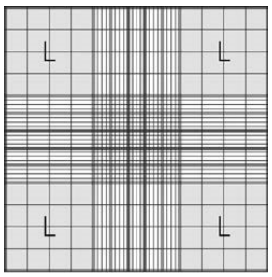

(b) Grid observed in the microscope. Cells in the four lateral squares labeled 'L' are counted to obtain cell number per ml

Figure 3.1: Hemocytometer (or Neubauer chamber) allows counting the number of cells in suspension

The procedure works as follows: 10 μl of the 1 ml solution with the cells and the medium is injected between the glass hemocytometer and the coverslip. The surface of the device is patterned with a squared grid, as shown in figure 3.1. Using the optical microscope, the cells inside the grid are counted and averaged (per square). This calculation is afterwards multiplied by 10,000 and the result is the number of cells per ml. Note that if the solution injected in the hemocytometer was previously diluted, the result of these calculations must be readjusted to reverse this dilution.

Afterwards, the resuspended cells are pipetted into the channels and the seeding is left to culture in the humidified incubator overnight. A part of the resuspended cells are returned to the flask and left to grow. The tests will be performed when a confluent monolayer of HCAECs in the channels is formed.

3.2 Flow test

In order to begin with the flow tests, the tubing system has previously been sterilised in the autoclave and the confluent monolayer of HCAECs has been cultured.

The system consists of a peristaltic pump, a set of tubes, a 5 ml bottle filled with cell medium and the microfluidic device assembled on a glass slide.

Firstly, control images of the cells along the three channels are taken in the phase-contrast microscope (Leica, DMi8) to be later compared with the disposition of the cells once subjected to flow.

Afterwards, the tubes are connected to allow a progressive feeding of the system. The flow rate is initially low to facilitate visual checking of any possible leaks and not to drastically affect the cultured cells. Once the system is proven watertight, the flow rate is set to the test value and the kit is kept in the humidified incubator for 32 hours, a sufficient time-frame for cells to respond to flow.[35] Throughout this time, images of the cells will be taken in the phase-contrast microscope every 8 hours to obtain their time dependent response.

The flow rates selected for the experimental tests due to the WSS values they generate are shown in table 3.1.

Table 3.1: Flow rates (ml/min) used in the experimental tests and WSS generated

Flow rate	**High WSS (Pa)**	**Low WSS (Pa)**
2.5 ml/min	0.55	0.16
3.5 ml/min	0.77	0.23
4.5 ml/min	1	0.3

After this period of time, the system is moved again to the microscope to obtain the images of the cells under flow conditions. Finally, the kit is carefully disassembled

and the tubing system is thoroughly checked and set aside for sterilisation and reutilisation. Cells must finally be fixed for immunostaining. This fixation consists in emptying and washing the device after the tests, to afterwards include a 4% paraformaldehyde (PFA) in PBS solution. It is then left at room temperature for 15 minutes. Finally, the solution is removed and the glass slide is kept submerged in PBS at 4ºC.

The immunostaining is out of the scope of this project. However, the cells here experimented will be fixed and kept as it will be performed to obtain more information about the morphology of the cytoskeleton.

3.3 Results

Two batches of experiments have been carried out so far. All the tests are detailed below. From the first batch, it was noted that a larger quantity of cells should be seeded in the devices, as the confluent monolayer needed for the experiments takes more time to grow than expected. This is due to the fact that the information regarding the number of cells per cm^2 obtained in literature was for HUVECs, which have higher growth rate. This modification was included in the second batch.

In the first batch, a total of four microfluidic devices were used. In table 3.2, the characteristics of each experiment are detailed.

Table 3.2: Test conditions of the first batch of experiments

Device	**Seeded cells/cm^2**	**Flow rate (ml/min)**	**High/Low WSS (Pa)**
1B	68,000	2.5	0.55 / 0.16
2B	68,000	3.5	0.77 / 0.23
3B	68,000	Static	Control
4B	97,000	4.5	1 / 0.3

Each device has three channels and all are subjected to the same flow rate, that is, the same shear stress levels.

In this second batch, only two devices were used due to cell availability, as can be seen in table 3.3. In order to obtain more information with only these two devices, one channel of each was left as static control.

Table 3.3: Test conditions of the second batch of experiments

Device	Seeded cells/cm^2	Flow rate (ml/min)	High/Low WSS (Pa)
7B	139,000	2.5 / Channel 2 static	0.55 / 0.16
12B	105,000	3.5 / Channel 3 static	0.77 / 0.23

To sum up, table 3.4 shows the total number of channels that have been subjeted to the different values of WSS.

Table 3.4: Number of channels per WSS value from all experiments

WSS (Pa)	Number of channels
0 - Control	5
0.16	5
0.23	5
0.30	3
0.55	5
0.77	5
1	3

Figures 3.2 and 3.3 show different stages of the experimental process that has been carried out.

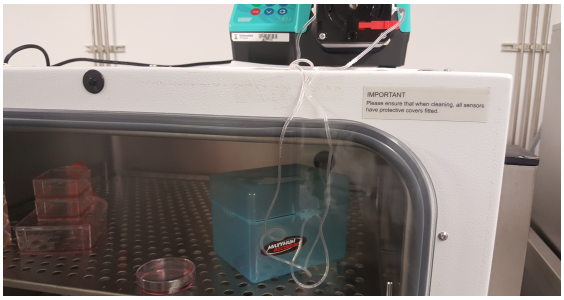

(a) System kept in the incubator. A box is used to keep the devices in order to contain water condensation

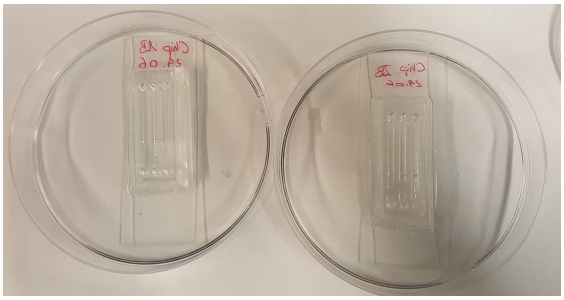

(b) Devices 1B and 2B after the tests, during the process of fixation once the medium is removed

Figure 3.2: Experimental montage and devices after usage

Once all phase-contrast images of the cells are gathered and analysed, the postprocessing of the results is performed in Matlab.

On another note, it is interesting to have a control culture of HUVECs, the common cell line used in bibliography, to justify the use of HCAECs and to validate the methodology of this work by comparing the results. This was performed along

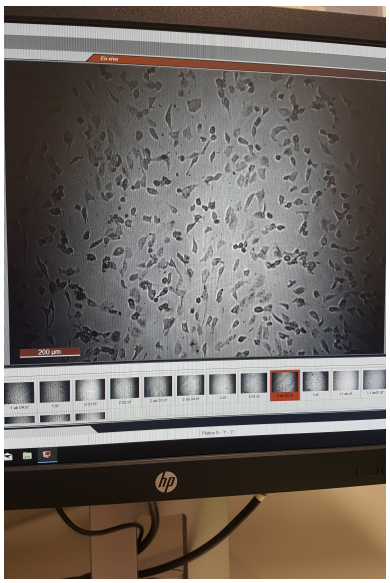

(a) The phase-contrast image acquisition

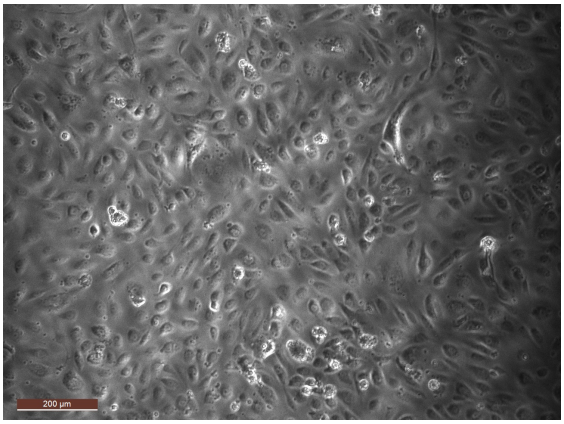

(b) Monolayer of HCAECs as seen in the phase-contrast microscope

Figure 3.3: Acquisition of phase-contrast images and the image itself

with the second batch of experiments. 200,000 cells/cm^2 were seeded and a very dense monolayer of HUVECs was formed. The amount of cells was so large throughout the whole experiment, that cells mounted on each other (see figure 3.4) and the phase-contrast images were impossible to decipher with the methodology here implemented. After these results, it has become clear that less amount of HUVECs has to be initially seeded.

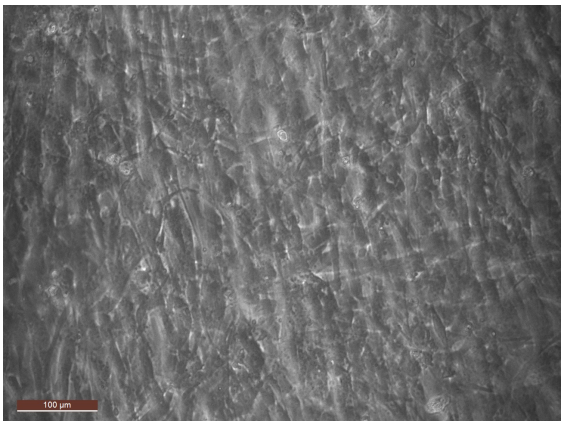

(a) HUVECs at the beginning of the tests

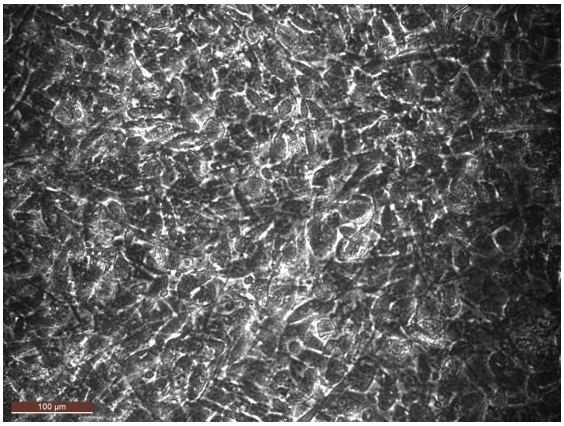

(b) HUVECs after 32h at 2.5 ml/min

Figure 3.4: Phase-contrast images of a monolayer of HUVECs. Cell monolayer is so dense that cell contours cannot be distinguished

Chapter 4

Image analysis and postprocessing of the results

Once the experimental test is finished, what remains to be processed are the grayscale microscope images of the cells throughout the experiment. From them, the information that must be extracted is the shape index (SI) of the cells and their orientation. The SI is a parameter that provides information about the circularity of the cells. A value of SI of 1 means a perfect circle, while a value closer to 0 means a more elongated shape, as can be inferred from equation (4.1). The orientation is calculated as the angle between the dominant direction of the cell and the direction of flow. These two factors will be calculated with the open software Fiji (ImageJ). However, the images are not quite high quality and the software does not automatically find the cell contours. Therefore, a preprocessing is needed. This preprocessing of the images will be carried out in Matlab R2016a.

$$SI = \frac{4 \cdot \pi \cdot area}{(perimeter)^2} \tag{4.1}$$

Once the images are adequately processed, they are introduced in Fiji for analysis. This is also programmed to be automatic, via macro-scripts. The information extracted from Fiji will be the results of the work.

4.1 Image preprocessing

The process followed is detailed hereunder.

First, the histogram of the images is expanded in order to broaden the grayscale range and increase differences and detail. Afterwards, the images are inverted using the function *imcomplement*, since it is better for the postprocessing to have darker background. Subsequently, the background of the images is estimated with the function *imopen* and removed. This step is carried out because the brightness in the pictures is not the same in the centre and in the borders. In order not to lose the information of one of these two parts, this homogenisation in brightness is necessary. After that, a contrast enhancement is implemented, to sharpen the edges, using *imadjust*. Figure 4.1 shows the comparison between the initial image and the resulting one after this whole preprocessing.

This is all the image processing prior to the binarization. The binarization basically transforms a grayscale image into a black and white one. For this, it is necessary to establish a threshold to differentiate which gray level is white and which one is black. However, only by establishing a threshold, these images are still not properly binarized, since lighter areas represent background in some places of the image and cells in others. Since this is quite a common problem, certain methods, like the function *imbinarize*, include the so called adaptive threshold, which establishes a local threshold in the neighbourhood of each pixel. With this method, the binarization of the images is fairly accurate. Finally, residual noise from the images is erased establishing a minimum amount of pixels per item with the function *bwareaopen*, as shown in figure 4.2.

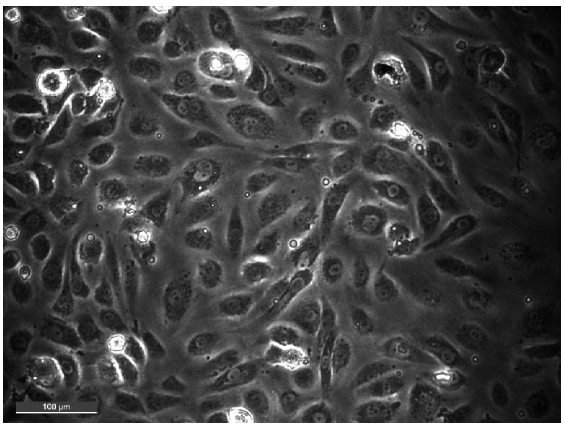

(a) Phase-contrast image of HCAECs. Darker areas can be seen in the left and right borders

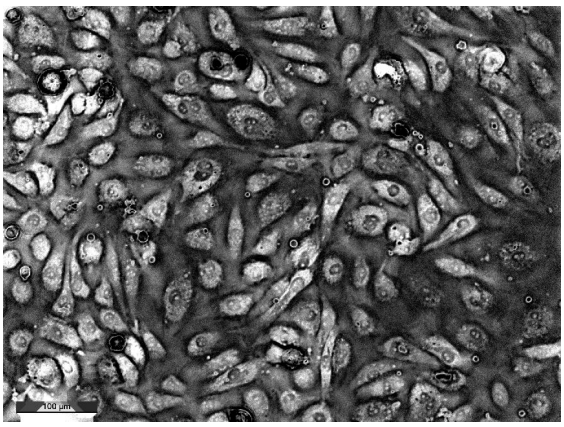

(b) Same image after preprocessing for binarization. It can be seen that cells in the edges have been recovered

Figure 4.1: Comparison in the preprocessing of images

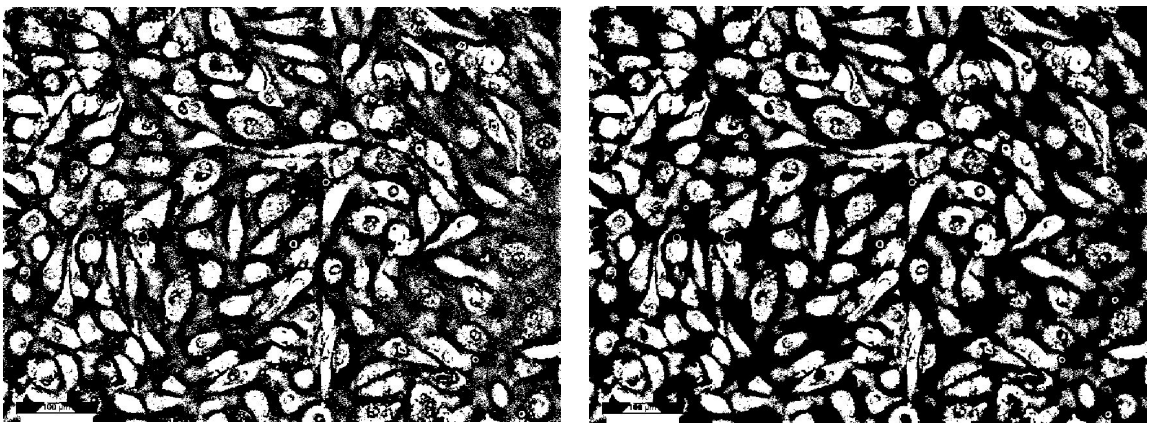

(a) Binarized image (b) Binarized image removing noise

Figure 4.2: Both steps in binarization

4.2 Particle analysis and measurement

The binarized images are imported to Fiji. This software allows batch processing through macro programming. However, before the measurement of SI and orientation, other preprocessing is carried out in this software.

Initially, a median filter is used. This filter replaces the value of the pixel for the median of itself and the adjacent neighbours. Since images are now black and white, the result of this filter is the smoothing of the contours.

After this, the option of filling holes in the image is applied. And finally, the particles are analysed in their geometrical parameters, with special interest in SI and orientation. In order not to count residual noise, a minimum pixel size limit is set. Similarly, since some cells have been left as an open geometry after all the processing, to not count this erroneous measurements a minimum shape index limit is established. These thresholds are set by a trial and error process. In figure 4.3, the result of the whole image analysis process is shown.

4.3 Results

Initially, every channel is studied separately to localise any misleading data. By doing this, an interesting pattern was found in the results. SI was expected to reduce (meaning that cells were elongating) in time, with its biggest reduction happening in the first time lapse.[35] This pronounced reduction can be seen in the first 8 hours of the tests. However, cells presented a sudden increase in SI from 16 to 24 hours that

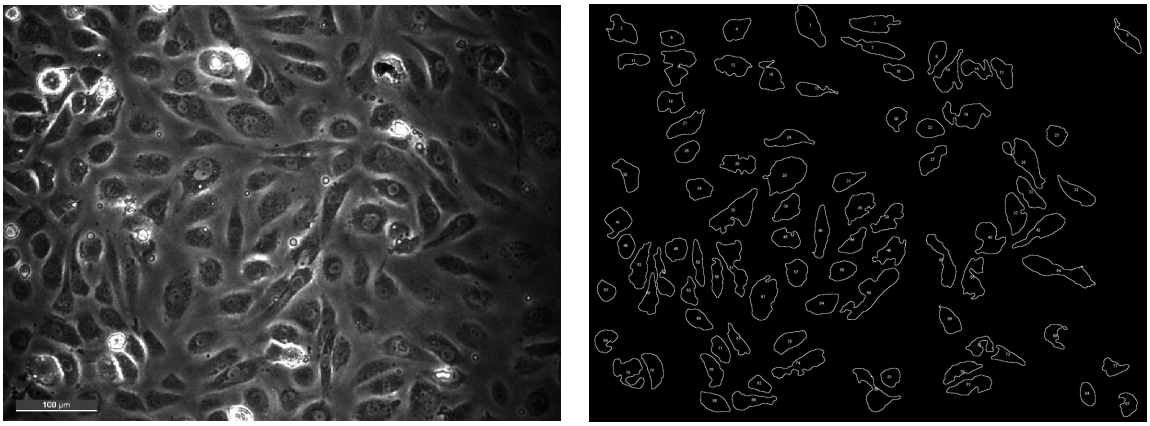

(a) Initial image (b) Cell contours detected by Fiji

Figure 4.3: Representation of the cell contours detection

prolonged until the end of the experiment, as can be seen in figure 4.4.

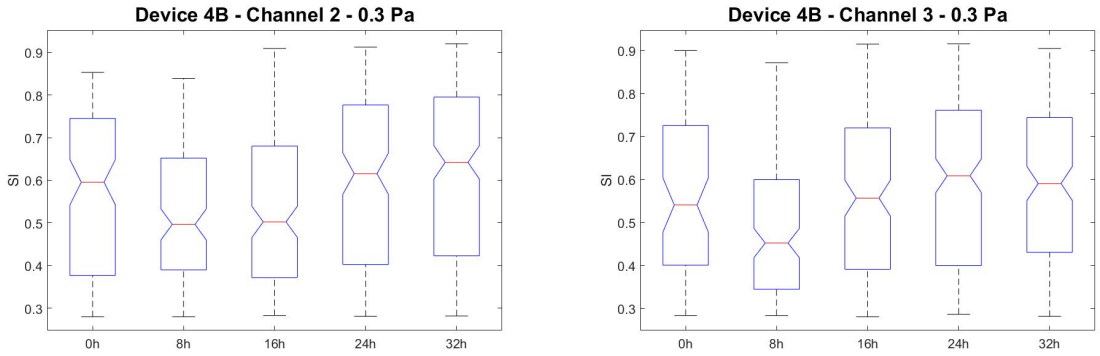

(a) SI increase 24h after beginning the test (b) SI increase 16h after beginning the test

Figure 4.4: Device 4B, representation of SI in two different channels, both subjected to 0.3 Pa

It is found that this unexpected increase in SI happens when many cells are seen to have detached. Figures 4.5 and 4.6 show the comparison between the channels 2 and 3 shown above before and after this detachment. It appears that, when cell density reduces and cells are far from forming a confluent monolayer, they return to a rounder shape. Apart from that, when cells are dying, they turn round before detaching. This could also alter the results of the experiment.

It becomes clear that a better adhesion and a confluent monolayer are needed for all these experiments. In fact, devices 7B and 12B, which were seeded with a larger quantity of cells (see table 3.3) and their monolayers were in better confluence, do not show this increase in SI, as shown in figure 4.7.

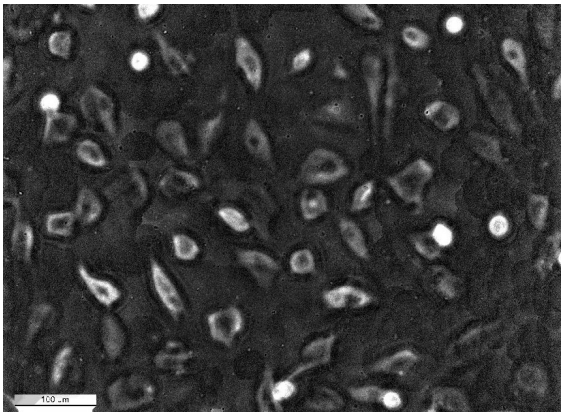

(a) 16 hours through the experiment

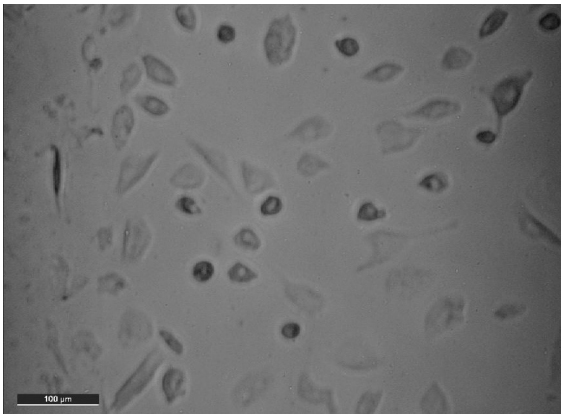

(b) 24 hours through the experiment

Figure 4.5: Device 4B, channel 2. Detachment of cells is seen 24 hours after the beginning of the flow test. Cells at this time show a rounder shape

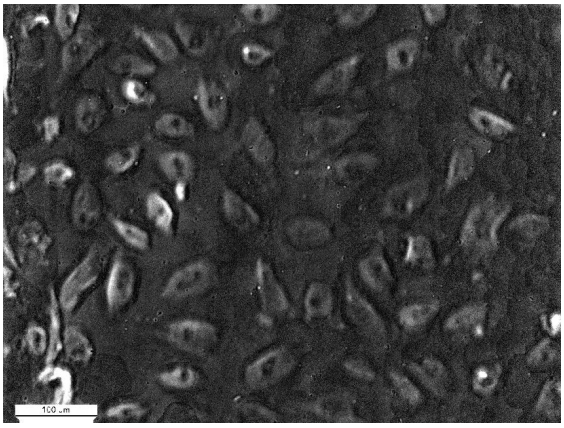

(a) 8 hours through the experiment

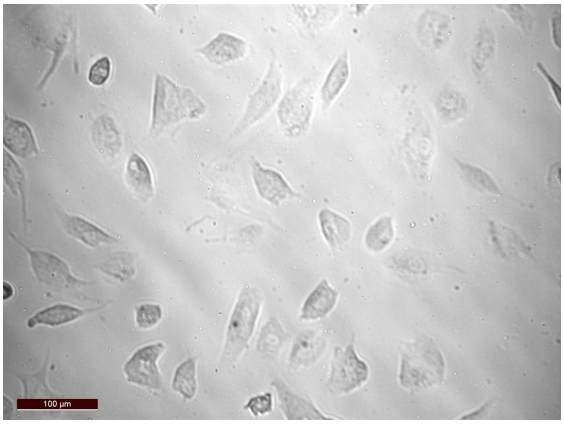

(b) 16 hours through the experiment

Figure 4.6: Device 4B, channel 3. Detachment of cells is seen 16 hours after the beginning of the flow test. Cells at this time show a rounder shape

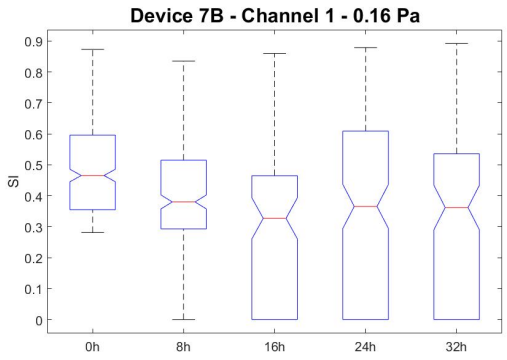

(a) SI in device 7B

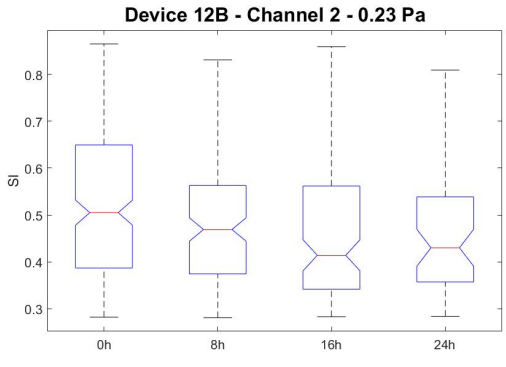

(b) SI in device 7B. No data in 32h as cells were infected

Figure 4.7: SI in devices 7B (left) and 12B (right). SI decreases progressively throughout the entire experiment

Considering all this information, results up to 8h are shown and analysed, except for the static conditions, where cells did not detach. This is acceptable considering literature, as most studies observe cell orientation in the first hours.[9,11,35]

However, this effect is taken into account for further experiments. Two modifications are already to be tested for the next batch of experiments in order to enhance cell adhesion. These are commented as future work of this project. Also, the number of cells per squared centimeter is also going to be increased, to vary between 150,000 and 200,000.

In the sections below, the results regarding cell shape and orientation, considering all commented above, are shown. All data have been clustered in the seven values of WSS studied, not specifying among devices or channels.

4.3.1 Cell shape

In order to evaluate the data, one-way analysis of variance (ANOVA) and t-tests are performed. The null hypothesis is that the means of the compared distributions are the same. A p value of 0.01 is chosen for all the tests.

First, the results of the static conditions are displayed in figure 4.8. Figure 4.9 shows the cells in static control at the beginning and at the end of the static experiment.

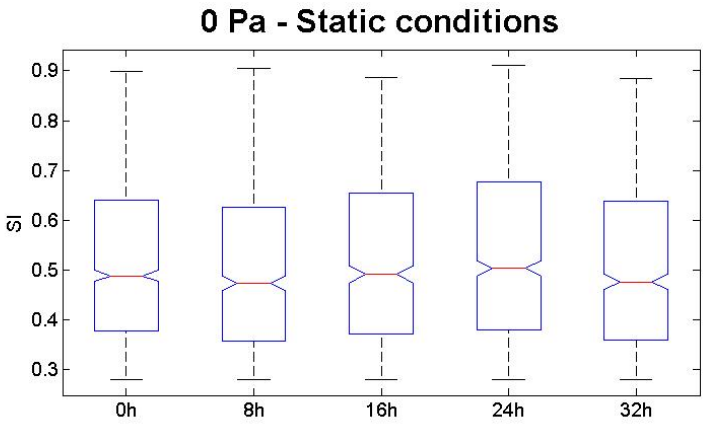

Figure 4.8: Shape index throughout the 32h of the experiments, for static conditions (0 Pa). No statistically significant difference was found between any set of data (p value>0.01)

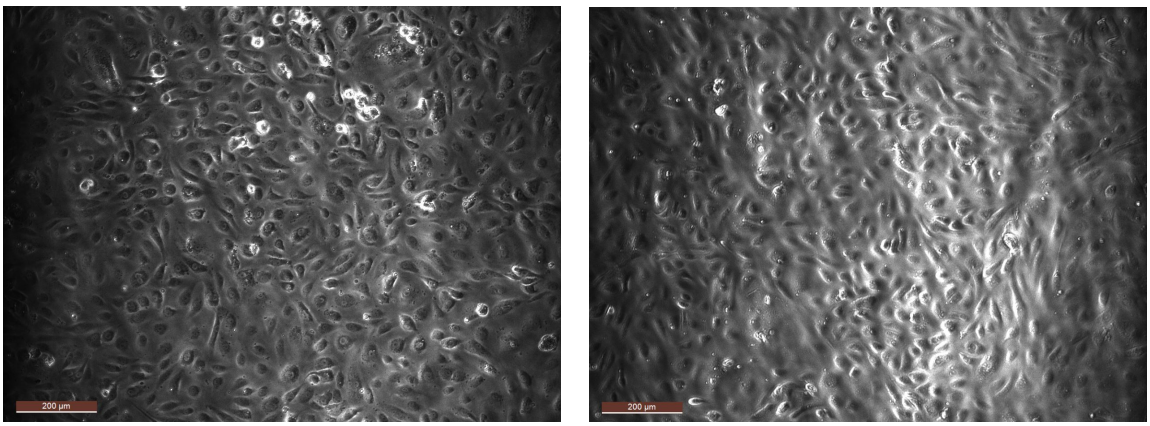

(a) Static control culture at the beginning (0h) (b) Static control culture after 32h

Figure 4.9: Device 12B, channel 3, cells in static control culture

Under static conditions, no statistically significant differences are found. The values of the medians range from 0.474 and 0.503, which represent quite elongated cells. These will be the values of reference to compare with the flow tests, as a static control of the specific cell type is essential.

Regarding the flow tests, figure 4.10 shows all the results obtained per WSS. For all values of WSS, a significant difference is obtained between cell shape at the beginning of the test and 8 hours into the experiment, see figure 4.11. Table 4.1 displays all the medians of the data, initially and after 8h.

Table 4.1: Median values of SI and percentage of decrease for all values of WSS tested, at the beginning of the experiments and after 8h. All decreases were found statistically significant with a p value of 0.01

	SI			
WSS (Pa)	**0h**	**8h**	**Decrease**	***p* value**
0.16	0.503	0.465	7.55%	$3.1 \cdot 10^{-8}$
0.23	0.505	0.475	5.94%	$3.2 \cdot 10^{-5}$
0.30	0.615	0.474	22.93%	$2.9 \cdot 10^{-11}$
0.55	0.489	0.441	9.82%	$1.3 \cdot 10^{-6}$
0.77	0.497	0.458	7.85%	$2.4 \cdot 10^{-3}$
1	0.481	0.432	10.19%	$4.9 \cdot 10^{-3}$

It can be noted that, except for the case of 0.3 Pa, all initial values match the tight range of SI of the control culture in static conditions. The final values of SI are also similar among all experiments, not presenting more elongation as WSS increases. As cell elongation has been obtained even for the smallest WSS value, a new group subjected to a lower WSS should be tested in the next batch.

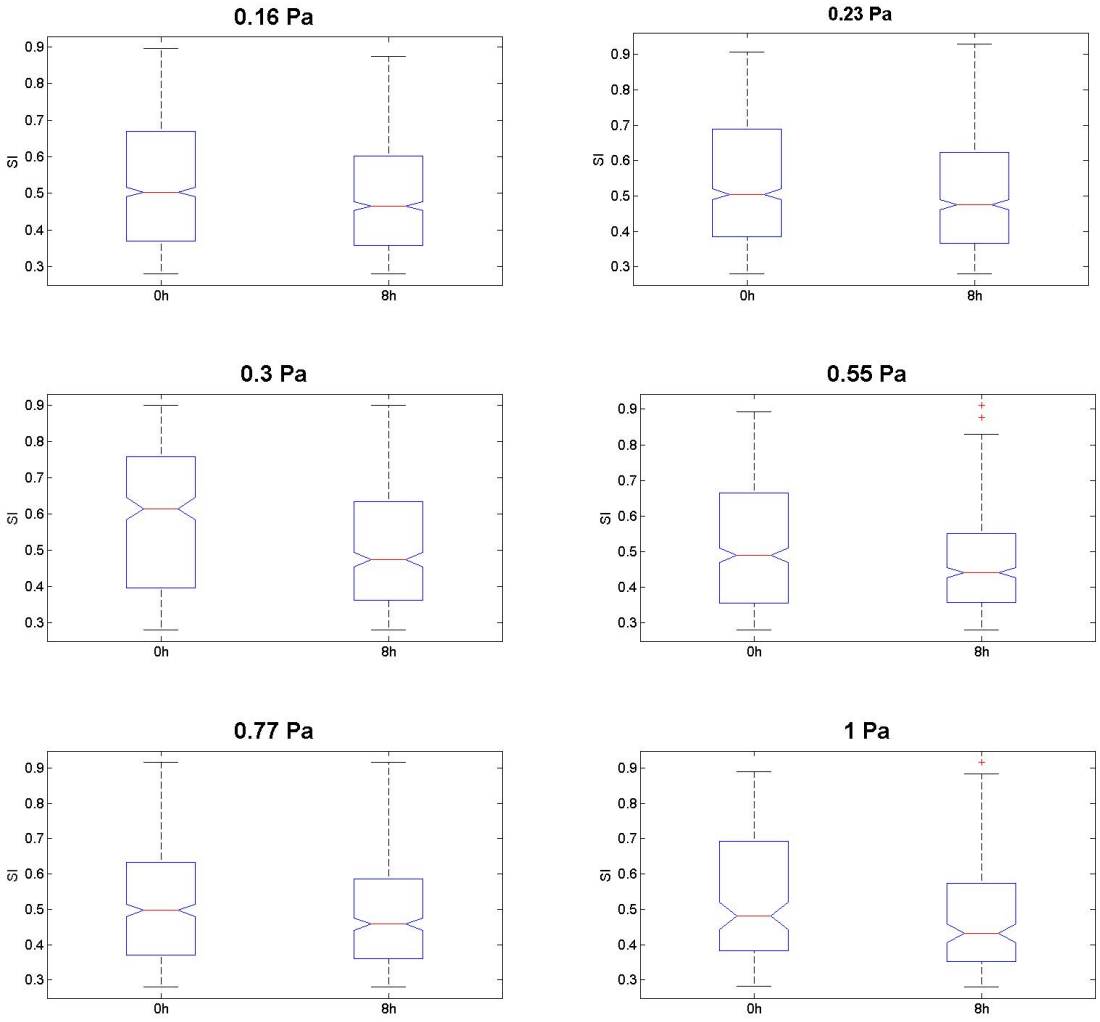

Figure 4.10: SI for all values of WSS, at the beginning of the experiments (0h) and 8 hours after. Statistically significant differences are found in all WSS cases

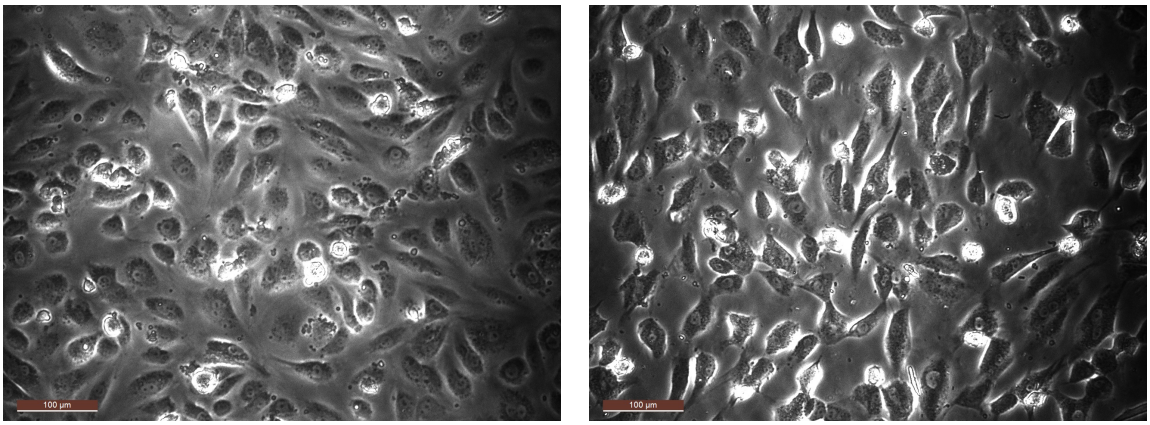

(a) Beginning of the flow test. Cells display a rounder shape

(b) 8 hours through the test. Cells appear more elongated

Figure 4.11: Device 12B, channel 2, cells subjected to 0.23 Pa (3.5 ml/min)

4.3.2 Cell orientation

Regarding cell orientation, the possible values range from -90º to 90º. At the beginning of the experiment, and under static conditions, a random orientation is expected. The mean or median in this case does not provide any information, since either a completely random or a fully oriented behaviour implies a mean value of 0º. A histogram, on the other hand, will display the distribution of results and allow a better understanding of cell behaviour. Figure 4.12 shows the histogram of orientations in the static conditions, in the initial moment and after 24 hours.

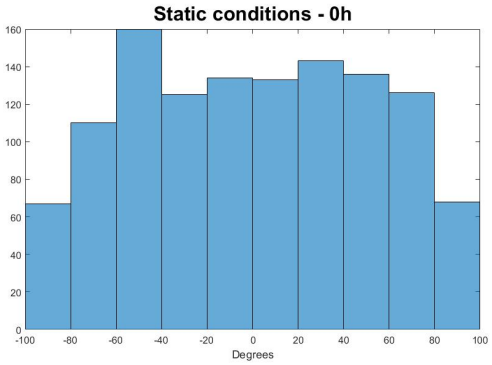

(a) Histogram for cell orientation at the beginning of the test in static conditions

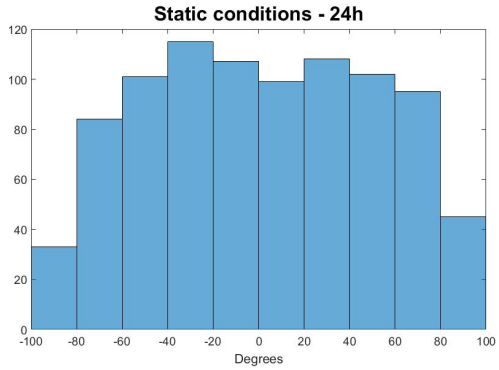

(b) Histogram for cell orientation 24 hours into the experiment in static conditions

Figure 4.12: Histograms for the orientation in static conditions at the beginning of the experiment and after 24 hours. An orientation of 0º indicates alignment with flow

A rather homogeneous distribution can be seen in both histograms, indicating no preferred orientation.

On the other hand, regarding the flow tests, an alignment with flow direction is expected, along with the elongation of cells. In figure 4.13, the histograms of different tests at the beginning and after 8 hours subjected to flow are shown.

In the initial conditions of all experiments, cell orientations show no preferred directions, inferred from a flat histogram. After 8 hours of flow conditions, cells become aligned with flow direction. This alignment can be perceived by the increase in the number of cells oriented around 0º, which represents the direction of flow. This happens in the cells subjected to a WSS of 0.23 Pa and higher, not appreciating a clear alignment in the case of 0.16 Pa.

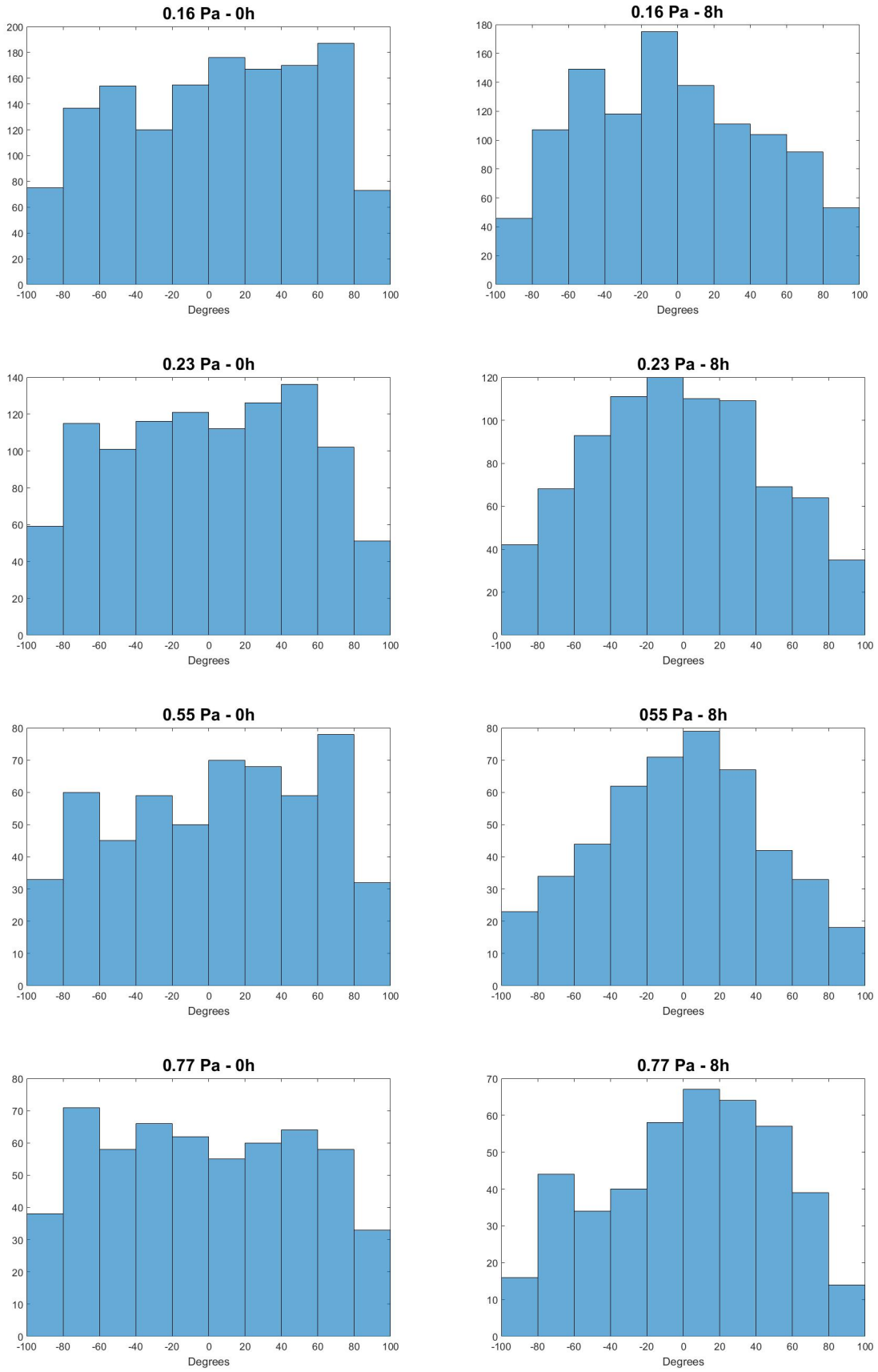

Figure 4.13: Histograms of cell orientation for three flow tests, at the beginning of the experiments (0h) and after 8 hours. Experiments subjected to 0.16, 0.23, 0.55 and 0.77 Pa are shown

Chapter 5

Discussion

ECs from vessel walls in the human body are constantly subjected to blood flow with different rates and, therefore, shear stresses. Cardiovascular diseases, like atherosclerosis, are highly localised, drawing attention to the biomechanical factors that can act as initiators. Because of this, flow tests with ECs are gaining attention in literature. These experiments can help understand the mechanisms of these pathologies, as cell response to flow remains an open subject.

There are several flow parameters that are altered in locations where atherosclerosis mainly appears. Among them, WSS has been thought to be the most relevant, due to its relation with wall permeability through ECs shape.

It is then the main objective of this work to correlate cell behaviour, in terms of shape and orientation, with WSS. To study this relation, a microfluidic device that reproduced the desired flow conditions has also been designed.

ECs have been shown to elongate and align with the flow, decreasing the permeability of the layer they are forming. However, depending on cell type, this response to flow starts at different values of WSS. Therefore, it is important to characterise properly the behaviour of every cell line. In this case, the use of HCAECs is especially interesting since the formation of the atheroma plaque in the coronary arteries is particularly dangerous, and they are not commonly studied in literature.

This study has successfully developed the conditions in which HCAECs modify their shape in response to flow. By comparing the results with the control cell culture in static conditions, cell elongation and orientation were obtained in all flow rates of the experiments, even with the smallest WSS.

Most flow studies with ECs use HUVECs or BAECs. They all report cell elongation in the presence of flow (WSS). However, the reported SI differs depending on cell type. Regarding HUVECs, Chiu et al.[7] reported a SI of 0.56 in the static conditions, achieving an elongation after exposed to 2.1 Pa of WSS, reaching a SI of 0.34. On the other hand, the results on BAECs show noticeable differences. Helmlinger et al.[35] reported an initial SI of around 0.8, meaning a very round shape of the cells. After 22h of flow and WSS of 1 Pa, the SI reduces its value to 0.5, where it remained for the following 24 hours of flow. However, Truskey et al.,[9] also working with BAECs, did not perceive a dramatic modification in SI after 24 hours of flow. They reported an initial SI of 0.44, which remained in the areas where flow is laminar and unidirectional.

Only one other study in literature has subjected HCAECs to shear stress (1 Pa), however only for 30 minutes.[11] Meza et al. show cell shape before and after their experiment in figure 5.1.

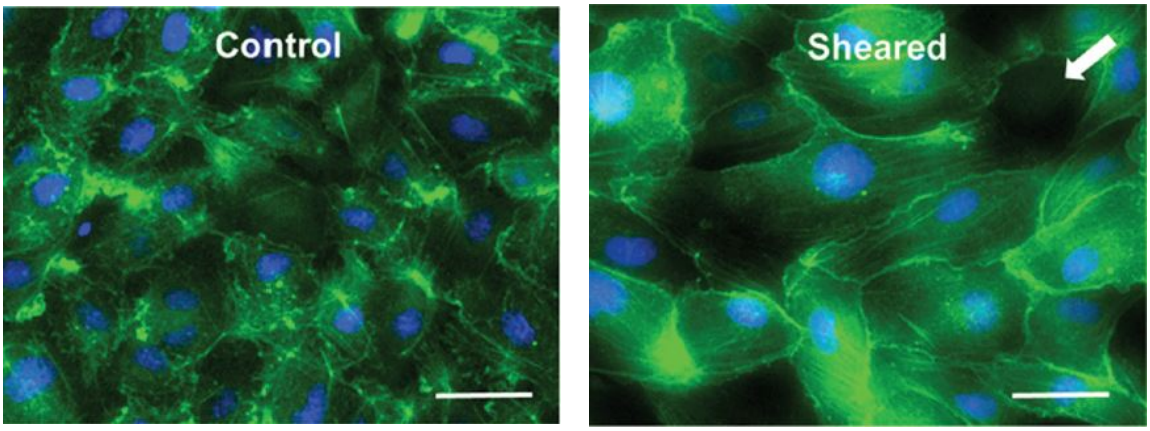

(a) Static control of HCAECs. Cells show a polygonal shape and no preferred orientation

(b) HCAECs after 30 minutes of a WSS of 1 Pa. White arrow indicates direction of WSS

Figure 5.1: Immunostained HCAECs in static control and subjected to 1 Pa of shear stress for 30 minutes

From these images, the SI and orientation of their cells are obtained. Numerical results regarding cell shape and orientation are not reported in this study. Therefore, all the information has been obtained from these two images. SI for the static control is 0.804 with a very small dispersion of data, ranging between 0.61 and 0.89. Regarding cell orientation, the histogram is very homogeneous throughout the whole range of possible directions, meaning a random distribution of the cells. Out of 14 measurements, 7 are in the range of -90º to 0º and the other 7 from 0º to 90º, with a mean in -0.09º. Regarding the sheared conditions, SI is reduced to 0.64, a reduction of

19%. The histogram of cell orientation now changes, with most orientations varying between -45º and 45º. Therefore, cell elongation and orientation is perceived in these results.

The results of the current work, although homogeneous and consistent, do not match completely the results reported in literature. Cells in this study show a noticeably more elongated shape in the static conditions than the other experiment on HCAECs. The percentage of elongation is therefore smaller in this study, as cells start already elongated. As the type of device is different in both studies (longitudinal channels vs cone-and-plate device), the static conditions in which cells are cultured do not match, noting the possibility of cells adapting their shape to the geometry of their environment. Regarding cell orientation, HCAECs in this work show alignment with flow direction, as all other studies in literature report. It was expected that the results would differ from those of other cell types. Taking into account the variations obtained in literature, the differences here found are considered acceptable.

Chapter 6

Conclusions

The objective of this study of designing and performing a flow test with HCAECs at different WSS values was successfully achieved. A redesign of the microfluidic device was needed to achieve the desired conditions, which facilitates further modifications in the geometry of the device.

Although the experiment was designed for 32 hours, considering cells would keep adjusting their behaviour, the relevant data was obtained from the first 8 hours of the experiment. This can be due to cell detachment after these 8 hours. Modifications are going to be implemented to prevent this detachment. However, it has been noted that testing time can be reduced, as the main response happens in the first hours.

Cell elongation was obtained in all experiments under shear stress conditions, even for the smallest value. Cell orientation, however, did not occur for the smallest WSS value, but did for the rest. It was expected to find the threshold from which cells start to modify their morphology considering the large range of WSS values covered. However, considering the results from this work, the threshold from which HCAECs start to elongate is still to be found.

In order to automate cell shape and orientation, an image analysis program has been successfully developed for phase-contrast images of ECs.

6.1 Future work

As commented above, this is a work in progress. Therefore, there are some modifications that are to be implemented promptly. There are also other worklines that have already been addressed. And, of course, there are bigger lines and

modifications for the future of this research.

In order to reduce cell detachment, there are a couple of modifications of the protocol that are going to be tested in the next batch of experiments. These are:

- The inclusion of a pulse damper in the flow system. The first pulse generated by the peristaltic pump is especially aggressive for the cells located near the entrance, mainly. Although this effect is attempted to be softened by beginning the tests with a low flow and progressively increasing it, detachment is still observed.

  A pulse damper basically consists of a deposit with a gas and a fluid cavity. When the fluid pulse enters, the gas absorbs it by its deformation, provoking an output of steady flow.

  This system is going to be implemented in the tube after the peristaltic pump.

- The adhesion treatment. Although collagen is used in literature for treating glass surfaces, fibronectin is also broadly used as adhesion protein in microfluidics.[7,37]

  In order to avoid cell detachment in the last hours of the experiment, this different treatment will be tried and compared with collagen.

Apart form that, the immunostaining of the fixed cells of the tests is still pending. It is expected that this technique will allow better observation of cell shape and orientation, as well as adhesion molecules and reactive oxygen species, which can also be related to the apparition of the plaque. However, this staining can only be performed when the experiment is over. Therefore, the information about the variation through time would be lost, so it is important to be able to obtain this information through the phase-contrast images.

Regarding further steps of the investigation, an update of the microfluidic device to include the step to provoke the recirculation is needed. This area has already been worked on and the step is already designed, as well as the mould for this geometry, which is already manufactured, see figure 6.1. Once cell attachment is resolved, the step will be included in all the channels of the devices.

Finally, this work is part of a PhD thesis. This project includes the determination of cell response to strain and to the coupled stimulus of stress and strain. These studies will need a new design for the device to allow applying a controlled strain in the substrate where cells are seeded.

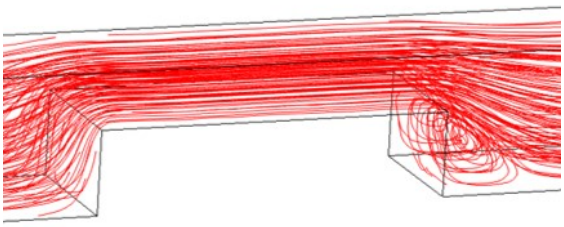

(a) Step and recirculation it provokes downstream

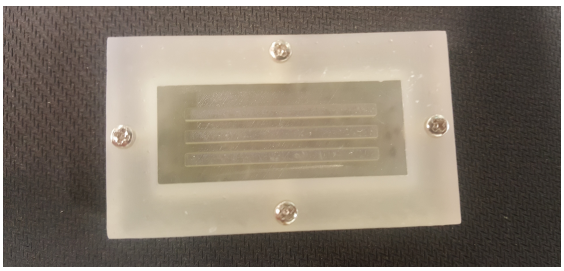

(b) Mould to fabricate the steps to be attached to the device

Figure 6.1: Recirculation area generated by the step and mould to fabricate such step

These results and the related further investigation will provide experimental correlations to a multiphysics computational model to predict atheroma plaque formation and development. Cell shape and alignment as a function of flow parameters will be translated into permeability of the endothelial layer and included in the equations that model the flux through the vessel wall.

Chapter 7

Bibliography

[1] J. S. VanEpps and D. A. Vorp. Mechanopathobiology of atherogenesis: A review. *Journal of Surgical Research*, 142(1):202–217, 2007.

[2] Canadian ultrasound institute - linkedin. `https://ca.linkedin.com/in/canadian-ultrasound-institute-93b798163`. Accessed: 2019-05-30.

[3] K. Islam, S. B. H. Timraz, R. Nasser, D. L .Gater, Y. E. Pearson, N. Christoforou, and J. C. M. Teo. Co-culture methods used to model atherosclerosis in vitro using endothelial, smooth muscle and monocyte cells. *SM Journal of Biomedical Engineering*, 2(1):1008–100815, 2016.

[4] J. J. Wentzel, Y. S. Chatzizisis, F. J. H. Gijsen, G. D. Giannoglou, C. L. Feldman, and P. H. Stone. Endothelial shear stress in the evolution of coronary atherosclerotic plaque and vascular remodelling: current understanding and remaining questions. *Cardiovascular Research*, 96(2):234–243, 2012.

[5] G. Dai, M. R. Kaazempur-Mofrad, S. Natarajan, Y. Zhang, S. Vaughn, B. R. Blackman, R. D. Kamm, G. Garcia-Cardena, and M. A. Gimbrone. Distinct endothelial phenotypes evoked by arterial waveforms derived from atherosclerosis-susceptible and -resistant regions of human vasculature. *Proceedings of the National Academy of Sciences*, 101(41):14871–14876, 2004.

[6] J.-J. Chiu and S. Chien. Effects of disturbed flow on vascular endothelium: Pathophysiological basis and clinical perspectives. *Physiological Reviews*, 91(1):327–387, 2011.

[7] J.-J. Chiu, D. L. Wang, S. Chien, R. Skalak, and S. Usami. Effects of disturbed flow on endothelial cells. *Journal of Biomechanical Engineering*, 120(1):2–8, 1998.

[8] F. Tovar-Lopez, P. Thurgood, C. Gilliam, N. Nguyen, E. Pirogova, K. Khoshmanesh, and S. Baratchi. A microfluidic system for studying the effects of

disturbed flow on endothelial cells. *Frontiers in Bioengineering and Biotechnology*, 7:1–7, 2019.

[9] G. A. Truskey, K. M. Barber, T. C. Robey, L. A. Olivier, and M. P. Combs. Characterization of a sudden expansion flow chamber to study the response of endothelium to flow recirculation. *Journal of Biomechanical Engineering*, 117(2):203–210, 1995.

[10] B. R. Blackman, G. García-Cardena, and Jr. M. A. Gimbrone. A new in vitro model to evaluate differential responses of endothelial cells to simulated arterial shear stress waveforms. *Journal of Biomechanical Engineering*, 124(4):397–407, 2002.

[11] D. Meza, L. Abejar, D. A. Rubenstein, and W. Yin. A shearing-stretching device that can apply physiological fluid shear stress and cyclic stretch concurrently to endothelial cells. *Journal of Biomechanical Engineering*, 138(3):031007–0310078, 2016.

[12] W. Zheng, B. Jiang, D. Wang, W. Zhang, Z. Wang, and X. Jiang. A microfluidic flow-stretch chip for investigating blood vessel biomechanics. *Lab on a Chip*, 12(18):3441–3450, 2012.

[13] N. V. Menon, H. M. Tay, K. T. Pang, R. Dalan, S. C. Wong, X. Wang, K. H. H. Li, and H. W. Hou. A tunable microfluidic 3D stenosis model to study leukocyte-endothelial interactions in atherosclerosis. *APL Bioengineering*, 2(1):016103–01610312, 2018.

[14] X. Zhang, D. J. Huk, Q. Wang, J. Lincoln, and Y. Zhao. A microfluidic shear device that accommodates parallel high and low stress zones within the same culturing chamber. *Biomicrofluidics*, 8(5):054106–05410612, 2014.

[15] M. J. Levesque and R. M. Nerem. The elongation and orientation of cultured endothelial cells in response to shear stress. *Journal of Biomechanical Engineering*, 107(4):341–347, 1985.

[16] E. A. Osborn, A. Rabodzey, C. F. Dewey, and J. H. Hartwig. Endothelial actin cytoskeleton remodeling during mechanostimulation with fluid shear stress. *American Journal of Physiology-Cell Physiology*, 290(2):C444–C452, 2006.

[17] L. Chau, M. Doran, and J. Cooper-White. A novel multishear microdevice for studying cell mechanics. *Lab on a Chip*, 9(13):1897–1902, 2009.

[18] R. M. Nerem. Shear force and its effect on cell structure and function. *ASGSB Bulletin*, 4(2):87 – 94, 1991.

[19] Y. Mohamied, E. M. Rowland, E. L. Bailey, S. J. Sherwin, M. A. Schwartz, and P. D. Weinberg. Change of direction in the biomechanics of atherosclerosis. *Annals of Biomedical Engineering*, 43(1):16–25, 2014.

[20] P. Sáez, M. Malvè, and M.A. Martínez. A theoretical model of the endothelial cell morphology due to different waveforms. *Journal of Theoretical Biology*, 379:16–23, 2015.

[21] P.-A. Doriot, P.-A. Dorsaz, L. Dorsaz, E. De Benedetti, P. Chatelain, and P. Delafontaine. In-vivo measurements of wall shear stress in human coronary arteries. *Coronary Artery Disease*, 11(6):495–502, 2000.

[22] ASTM D638-14. Standard test method for tensile properties of plastics. Standard, American Society for Testing and Materials, December 2014.

[23] UNE-EN ISO 527-1. Plásticos. determinación de las propiedades en tracción. parte 1: Principios generales. Technical report, Asociación Española de Normalización y Certificación, November 2012.

[24] Y. Huo, J. S. Choy, M. Svendsen, A. K. Sinha, and G. S. Kassab. Effects of vessel compliance on flow pattern in porcine epicardial right coronary arterial tree. *Journal of Biomechanics*, 42(5):594–602, 2009.

[25] M. B. Dancu, D. E. Berardi, J. P. Vanden Heuvel, and J. M. Tarbell. Asynchronous shear stress and circumferential strain reduces endothelial NO synthase and cyclooxygenase-2 but induces endothelin-1 gene expression in endothelial cells. *Arteriosclerosis, Thrombosis, and Vascular Biology*, 24(11):2088–2094, 2004.

[26] Y. Qiu and J. M. Tarbell. Interaction between wall shear stress and circumferential strain affects endothelial cell biochemical production. *Journal of Vascular Research*, 37(3):147–157, 2000.

[27] Y. Tardy, N. Resnick, T. Nagel, M.A. Gimbrone, and C.F. Dewey. Shear stress gradients remodel endothelial monolayers in vitro via a cell proliferation-migration-loss cycle. *Arteriosclerosis, Thrombosis, and Vascular Biology*, 17(11):3102–3106, 1997.

[28] L. Rouleau, J. Rossi, and R. L. Leask. Concentration and time effects of dextran exposure on endothelial cell viability, attachment, and inflammatory marker expression in vitro. *Annals of Biomedical Engineering*, 38(4):1451–1462, 2010.

[29] A. R. Wechezak, D. E. Coan, R. F. Viggers, and L. R. Sauvage. Dextran increases survival of subconfluent endothelial cells exposed to shear stress. *American Journal of Physiology-Heart and Circulatory Physiology*, 264(2):H520–H525, 1993.

[30] F. Carrasco, E. Chornet, R. P. Overend, and J. Costa. A generalized correlation for the viscosity of dextrans in aqueous solutions as a function of temperature, concentration, and molecular weight at low shear rates. *Journal of Applied Polymer Science*, 37(8):2087–2098, 1989.

[31] A. K. Au, W. Huynh, L. F. Horowitz, and A. Folch. 3D-printed microfluidics. *Angewandte Chemie International Edition*, 55(12):3862–3881, 2016.

[32] B. Gale, A. Jafek, C. Lambert, B. Goenner, H. Moghimifam, U. Nze, and S. Kamarapu. A review of current methods in microfluidic device fabrication and future commercialization prospects. *Inventions*, 3(60):1–25, 2018.

[33] T. Pravinraj and R. Patrikar. Modeling and characterization of surface roughness effect on fluid flow in a polydimethylsiloxane microchannel using a fractal based lattice boltzmann method. *AIP Advances*, 8(6):065112–0651126, 2018.

[34] P. F. Costa, H. J. Albers, J. E. A. Linssen, H. H. T. Middelkamp, L. van der Hout, R. Passier, A. van den Berg, J. Malda, and A. D. van der Meer. Mimicking arterial thrombosis in a 3D-printed microfluidic in vitro vascular model based on computed tomography angiography data. *Lab on a Chip*, 17(16):2785–2792, 2017.

[35] G. Helmlinger, R. V. Geiger, S. Schreck, and R. M. Nerem. Effects of pulsatile flow on cultured vascular endothelial cell morphology. *Journal of Biomechanical Engineering*, 113(2):123–131, 1991.

[36] W. Zheng, R. Huang, B. Jiang, Y. Zhao, W. Zhang, and X. Jiang. An early-stage atherosclerosis research model based on microfluidics. *Small*, 12(15):2022–2034, 2016.

[37] R. Estrada, G. A. Giridharan, M.-D. Nguyen, S. D. Prabhu, and P. Sethu. Microfluidic endothelial cell culture model to replicate disturbed flow conditions seen in atherosclerosis susceptible regions. *Biomicrofluidics*, 5(3):032006–03200611, 2011.

List of Figures

List of Tables